International Journal of Mining Science and Technology 35 (2025) 1789–1807

Contents lists available at ScienceDirect

International Journal of Mining Science and Technology

journal homepage: www.elsevier.com/locate/ijmst

Flow behavior of a rough single rock fracture under high-temperature, high-stress, and high-seepage pressure coupling conditions

Bingqi Wang [a,b], Wendong Yang [a,b,*], Xiang Zhang [a,b], Yongfei Yang [a,c], Lei Zhang [a,c], Jun Yao [a,c]

[a] State Key Laboratory of Deep Oil and Gas, China University of Petroleum (East China), Qingdao 266580, China
[b] College of Pipeline and Civil Engineering, China University of Petroleum (East China), Qingdao 266580, China
[c] College of Petroleum Engineering, China University of Petroleum (East China), Qingdao 266580, China

ARTICLE INFO

Article history:
Received 30 April 2025
Received in revised form 3 August 2025
Accepted 9 September 2025
Available online 4 October 2025

Keywords:
Coupled HTHM condition
Nonlinear flow
Rough single fracture
Improved Forchheimer equation

ABSTRACT

Understanding the complex flow behavior along a rough rock fracture under high-temperature, high-stress, and high-seepage pressure (HTHM) coupling conditions is of great significance for optimizing deep resource extraction. This study investigates the complex flow behavior of a single rock fracture under coupled HTHM conditions using a self-developed multi-field coupling experimental system, considering real-time high temperatures (20–90 °C), confining pressures (30–120 MPa), and seepage pressures (5–60 MPa). Experimental results show that as confining pressure increases, two typical nonlinear flow behaviors are observed, which are Forchheimer flow and low-velocity nonlinear flow. The increase in temperature and decrease in roughness significantly promote the fluid flow and enhance the nonlinear relationship between the volumetric flow rate and the hydraulic gradient at lower confining pressures (30 MPa). However, the change in temperature and fracture surface roughness does not affect the nonlinear type of fluid flow. Under a given hydraulic gradient, the influence of temperature and fracture roughness on the volumetric flow rate varies with changes in confining pressure. Additionally, this study considers both the viscous and inertial terms, and a modified Forchheimer equation is proposed using two parameters: the contact area ratio and the thermal expansion coefficient of the rock. The proposed model can effectively predict the nonlinear flow behavior of fluid along rough fractured rocks under varying temperatures and surface roughness. The experimental results and the proposed model provide valuable data and theoretical guidance for deep oil and gas exploration as well as hydraulic fracturing design.

1. Introduction

With the rapid development of global oil and gas industries, petroleum exploration has progressively extended into deep (4500–6000 m) and ultra-deep (>6000 m) formations, which are regarded as critical frontiers for future energy development [1,2]. In China, substantial hydrocarbon resources have been continuously discovered in deep and ultra-deep carbonate reservoirs within the Tarim Basin, Sichuan Basin, and Ordos Basin [3]. According to the evaluation of China's oil and gas resources, the estimated deep and ultra-deep oil and gas resources amount to 67.1 billion tons of oil equivalent, accounting for 34% of China's total oil and gas resources [4]. The exploration and development of deep and ultra-deep oil and gas reservoirs play a crucial role in expanding reserves and ensuring energy security. As shown in Fig. 1, deep reservoirs are characterized by high temperatures (>100 °C, high in-situ stresses (>100 MPa), and high pressures (>50 MPa), with well-developed fracture networks [5]. Fluid flow behavior in reservoir fractures exhibits significant nonlinearity, yet its underlying mechanisms remain unclear, significantly increasing the development difficulty and cost of deep and ultra-deep oil and gas reservoirs [6]. Compared to the rock matrix, fluid flow behavior in rock fractures is more sensitive to temperature variations, in-situ stress states, and seepage pressure changes [7]. Fractures exhibit higher hydraulic conductivity and serve as the primary pathways for oil and gas storage and migration, directly influencing oil production efficiency. Therefore, a thorough understanding of fluid flow behavior in rough rock fractures under HTHM conditions is of great theoretical and practical significance for the efficient development of deep and ultra-deep large-scale oil and gas fields.

Existing studies have extensively investigated the effects of individual factors such as confining pressure, seepage pressure, and temperature on fluid flow behavior in fractures. Seepage experiments on rough single fractures under varying confining pressures have been conducted to analyze the relationship

* Corresponding author.
E-mail address: yangwd@upc.edu.cn (W. Yang).

https://doi.org/10.1016/j.ijmst.2025.09.001
2095-2686/

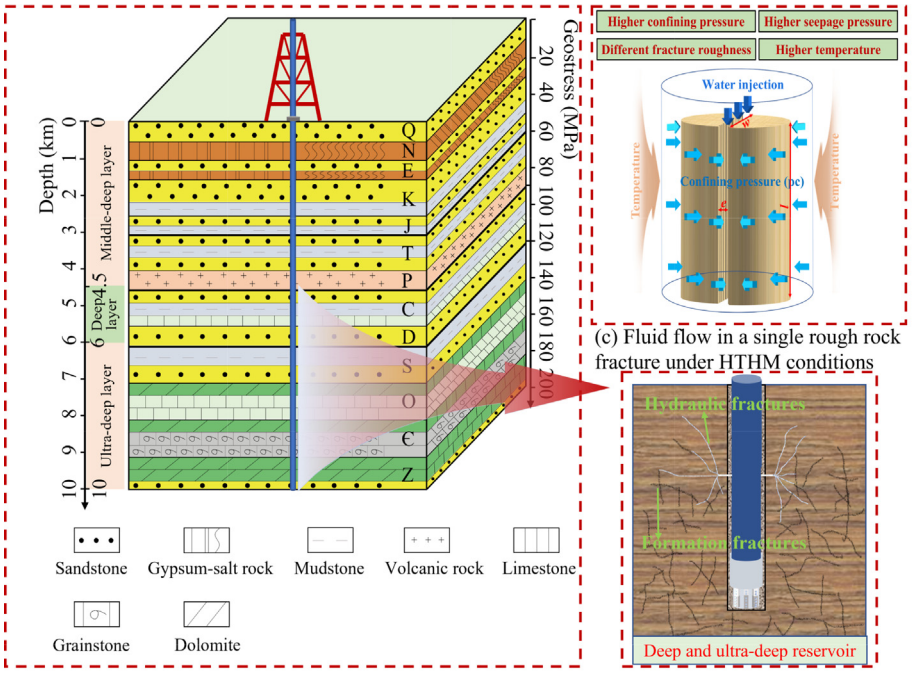

(a) Schematic diagram of key stratigraphy in Tarim Basin (b) Fractures in deep and ultra-deep stratigraphy

Note: Quaternary, Neogene, Paleogene, Cretaceous, Jurassic, Triassic, Permian, Carboniferous, Devonian, Silurian, Ordovician, Cambrian, and Sinian are labelled with Q, N, E, K, J, T, P, C, D, S, O, Є, and Z, respectively.

Fig. 1. Main stratigraphic distribution characteristics of the Tarim Basin.

between fracture aperture, hydraulic conductivity, and confining pressure. These studies have demonstrated that confining pressure directly reduces fracture aperture, thereby decreasing the fluid transport capacity within fractured rocks [8,9]. Seepage pressure is a critical factor influencing changes in fluid flow behavior. At low seepage pressure, fluid flow predominantly follows Darcy's law, exhibiting linear flow characteristics [10]. As seepage pressure increases, a nonlinear relationship between hydraulic gradient and volumetric flow rate emerges. Notably, elevated seepage pressure also affects fluid-solid interactions within the fracture, inducing phenomena such as shear slip and localized turbulence [11]. The increase in temperature not only alters the physical properties of the fluid but also induces thermal expansion of the rock matrix and redistribution of thermal stress, consequently influencing flow behavior in the reservoir. In addition to these factors, extensive experimental and numerical studies have demonstrated the significant impact of fracture roughness on fluid flow behavior. The greater the roughness, the more significant the fluctuation of the fracture surface, resulting in tortuous flow paths, reduced connectivity of flow channels, and a transition from linear to nonlinear flow [12]. Researchers have introduced various roughness parameters, including the joint roughness coefficient (JRC) [13], fractal dimension [14], relative roughness [15], average roughness of a profile [16], tortuosity [17], and contact ratio [18]. Based on these parameters, studies have examined flow behavior in rough rock fractures under different roughness conditions [19,20].

Based on extensive experimental research, it has been well recognized that the linear Darcy's law is insufficient to describe the nonlinear flow behavior of fluids in natural rock fractures [21]. The essence of nonlinear flow lies in the nonlinear relationship between fluid velocity and hydraulic gradient. Such nonlinearity typically arises from inertial effects at high flow velocities, disturbances caused by fracture surface roughness, and stress-induced fracture deformations. Among the various models developed to describe nonlinear fluid flow behavior, the cubic law and the Forchheimer equation are widely used to characterize non-Darcy flow in fractured media [22]. The cubic law is a fundamental equation used to describe fluid flow in fractures. It assumes that an incompressible Newtonian fluid flows steadily between two parallel plates, with the flow direction parallel to the plates. Although the cubic law neglects nonlinear fluid behavior and complex boundary conditions, it offers a straightforward formula for estimating volumetric flow rate. It remains relatively accurate in describing fracture flow under laminar conditions, and is therefore widely applied in groundwater flow analysis [23]. The Forchheimer equation, on the other hand, incorporates a quadratic velocity term into the classical Darcy's law to account for inertial effects at high flow rates, enabling a more accurate description of nonlinear flow behavior. Schrauf and Evans validated the theoretical applicability of the Forchheimer equation for fluid flow in fractured media through dimensional analysis [24]. Notably, the nonlinear coefficient in the Forchheimer equation is highly dependent on the geometrical characteristics of the fracture surface. As a result, modeling fluid flow in fractured rocks often focuses on the accurate determination of this nonlinear coefficient. In addition, several other models, such as the Darcy–Weisbach and Darcy–Forchheimer equations, have been proposed under different flow conditions and physical assumptions to further characterize nonlinear flow behavior [25]. However, the application of these models typically requires extensive experimental calibration under specific conditions, which significantly limits their practical implementation in engineering contexts.

As energy extraction progressively extends into the Earth's deep subsurface, the flow behavior of fluids in rock fractures under

thermo-hydro-mechanical (THM) coupling has attracted widespread attention. As shown in Table 1, several researchers have recently conducted experimental and theoretical studies on the flow behavior of fractured rock in a coupled THM environment. These studies have clarified that the coupled THM processes play a combined role in the flow behavior of fractured rocks. As shown in Fig. 1c, on the one hand, an increase in temperature reduces the dynamic viscosity of the fluid, decreases the fluid flow resistance, and modifies the flow behavior [26]. On the other hand, temperature increases cause thermal expansion and thermal stress in the rock, which alters the stress field and, in turn, affects the aperture of fractures and the flow path of fluids. Variations in the stress field lead to the closure or opening of fracture apertures, which further influence the distribution of the pressure field. Fluids flowing through fractures exert liquid pressure on the fractures, modifying the system's heat flux and subsequently affecting the stress and temperature fields in the rock. Due to the complex interactions within THM coupling, Darcy's law is no longer sufficient to describe the flow behavior of fluids in complex environments [27,28]. However, existing studies on flow behavior of fractured rock under THM coupling conditions have primarily focused on confining pressures not exceeding 60 MPa and seepage pressures of no more than 15 MPa, which significantly differ from the actual conditions of deep reservoirs [29,30]. There remains a lack of comprehensive and detailed investigations into the flow behavior of rough fractures under HTHM coupling.

In this study, the effects of temperature, confining pressure, and seepage pressure on the flow behavior of a single rough rock fracture are investigated, and the evolution of the flow characteristics in rough fractured rocks under HTHM coupling is analyzed. Additionally, the contact area ratio and the thermal expansion coefficient of the rock are introduced. An improved Forchheimer equation is proposed to accurately predict the flow behavior of fractured rocks in complex underground environments. This study aims to provide theoretical support and technical guidance for geothermal development, deep oil and gas extraction, and related fields, thereby promoting the application of relevant technologies.

2. Theoretical background and improved Forchheimer equation

The classic model for fluid flow through fractures is based on the assumption of smooth fracture surfaces and is defined as the cubic law [9]:

$$Q = -\frac{we_h^3}{12\mu}\nabla P \tag{1}$$

where Q is the volumetric flow rate; w the fracture width; e_h the hydraulic aperture, which is defined as the equivalent smooth aperture that has the same hydraulic conductivity as the original rough fracture; μ the dynamic viscosity of water; and ∇P the pressure gradient.

When fluid flows at high velocities, inertial effects become significant, leading to a deviation from the linear relationship between the volumetric flow rate and hydraulic gradient described by the Cubic law, thereby entering the non-Darcy flow regime. To describe the nonlinear fluid flow in fractured rock, the Forchheimer equation introduces a quadratic term based on the cubic law to quantify the influence of inertial effects on the flow. The Forchheimer equation has been widely validated for describing nonlinear fluid flow in porous media and fractured rock, and is typically expressed as follows [23]:

$$-\nabla P = \frac{12\mu}{we_h^3}Q + \frac{\beta\rho}{w^2e_h^2}Q^2 = aQ + bQ^2 \tag{2}$$

where a and b represent coefficients describing the pressure drops due to viscous effect and inertial effect, respectively; β the fitting coefficient of the nonlinear term; and ρ the density of water.

By measuring the non-Darcy coefficient β for different media through experiments and combining numerical simulation methods, the complex flow behavior of fluid in rock fractures under high velocities can be effectively analyzed [38]. Although the classical Forchheimer equation effectively describes nonlinear fluid flow in fractured rocks, its application in engineering practice is often limited by the need to calibrate experimentally its coefficients under specific boundary conditions. In deep underground engineering, environmental parameters such as temperature, stress, and seepage pressure vary significantly with depth. To ensure the traditional Forchheimer equation accurately captures fluid behavior at different depths, numerous experiments would be required to recalibrate the model coefficients for each set of conditions, which is both time-consuming and impractical. To overcome this limitation, we introduce two physically-based correction parameters, the thermal expansion coefficient and the contact area ratio, to modify the linear and nonlinear terms of the Forchheimer equation. The improved equation aims to enhance the model's predictive capability under varying temperature and fracture roughness conditions, without the need for exhaustive recalibration. Specifically, the thermal expansion coefficient accounts for temperature-induced changes in fracture aperture, which in turn affect the fluid's flow resistance. The contact area ratio, on the other hand, quantifies the effective contact area between rough fracture surfaces and reflects the influence of mechanical closure on the inertial resistance to flow. This parameter also addresses a known limitation of using the JRC in three-dimensional fracture analysis: different fracture geometries may yield the same JRC value, despite having distinct surface morphologies.

Table 1
Recent studies on the flow behavior of rocks under THM coupling conditions.

Temperature (°C)	Confining pressure (MPa)	Seepage pressure (MPa)	Research object	Reference
25–250	15	0–15	Fractured rock	Li et al. [31]
25–90	6	4	Pre–cracked rock	Yi et al. [32]
25–600	25	6	Marble	Meng et al. [30]
50–200	0–50	2	EGS fracture	Zhang et al. [33]
25–120	30	0.2	Single rock fracture	Wu et al. [34]
20–700	25	6	Salt rock	Liang et al. [29]
25–650	25	5	Salt rock	Meng et al. [35]
25–650	25	6	Fracture network	Wu et al. [36]
100	20	10	Reservoir rock	Huang et al. [37]

Studies have shown that in smooth fractures, temperature changes do not cause the fluid flow behavior to shift from linear to nonlinear. Therefore, to enable the improved Forchheimer equation to effectively predict fluid flow in fractures, it is essential to incorporate the influence of temperature on hydraulic aperture into the linear term of the traditional Forchheimer equation. The effect of temperature variation on fluid flow behavior in fractures is manifested in two aspects. First, an increase in temperature alters the fluid viscosity coefficient. Second, thermal expansion of the rock due to temperature rise modifies the hydraulic aperture. Considering the above effects, introducing the thermal expansion coefficient enables Eq. (3) to effectively predict the flow behavior of a single fracture under laminar conditions at different temperatures. In this study, the modified Cubic law was validated using the experimental data from Kumari and Ranjith [39]. Using the experimental data at 20 °C as a reference, Eq. (3) was applied to predict fluid flow behavior at 50 and 150 °C and the corresponding $-\nabla P$–Q curves were plotted. As illustrated in Fig. 2, the predicted values at 50 and 150 ℃ exhibit a strong correlation with the experimental data, with R^2 values exceeding 0.95. The coefficients $\left[\frac{\alpha(T_{20})}{\alpha(T_{50})}\right]^3$ and $\left[\frac{\alpha(T_{20})}{\alpha(T_{150})}\right]^3$ are 0.98 and 0.95, respectively [40]. Here, $\alpha(T_{20})$, $\alpha(T_{50})$, and $\alpha(T_{150})$ denote the thermal expansion coefficient of rock at 20, 50, and 150 °C, respectively. It should be noted that when maintaining the same temperature and a smooth plane condition, Eq. (3) can be simplified to the cubic law:

$$Q = -\frac{we_h^3}{12\mu}\nabla P\left[\frac{\alpha(T_0)}{\alpha(T)}\right]^3 \tag{3}$$

where $\frac{\alpha(T_0)}{\alpha(T)}$ represents the ratio of the thermal expansion coefficient of rock at the experimental temperature to that at the predicted temperature.

The relative coefficient of thermal expansion is defined as follows:

$$\eta = \frac{\alpha(T_0)}{\alpha(T)} \tag{4}$$

Based on Eqs. (3) and (4), the improved cubic law as in Eq. (5):

$$-\nabla P = \frac{12\mu}{we_h^3\eta^3}Q = AQ \tag{5}$$

where $e_h^3\eta^3$ reflects the decrease of hydraulic aperture due to thermal expansion after temperature rise.

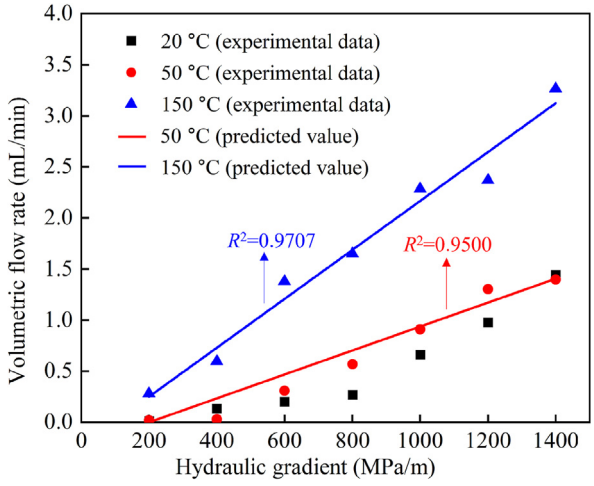

Fig. 2. Validation of the improved cubic law model considering temperature effects.

In view of the nonlinear flow behavior of fluid in a rough rock fracture, this study improves the nonlinear term in the Forchheimer equation by incorporating the effects of fracture surface roughness, contact area, and temperature on fluid flow. The JRC is one of the most widely used parameters for characterizing fracture surface geometry due to its intuitiveness and ease of experimental measurement [13]. Based on the description of the fracture geometry and a large number of laboratory experimental data, Barton et al. [41] pointed out that the hydraulic aperture and the mechanical aperture of the fracture are affected by the roughness. The greater the roughness, the lower the actual flow capacity of the fluid in the fracture.

$$e_h = e_m^2/\mathrm{JRC}^{2.5} \tag{6}$$

where e_m is the mechanical aperture.

Walsh [42] introduced the contact area ratio (ω) as a new parameter to characterize the roughness of fractured rock and proposed a relationship between the mechanical aperture, contact area ratio, and hydraulic aperture:

$$e_h^3 = \left(\frac{1-\omega}{1+\omega}\right)e_m^3 \tag{7}$$

By associating Eqs. (6) and (7), the relationship between hydraulic aperture, JRC, and contract area ratio are obtained:

$$e_h^2 = \left(\frac{1-\omega}{1+\omega}\right)^{\frac{4}{3}}\mathrm{JRC}^5 \tag{8}$$

By substituting Eq. (9) into the Forchheimer equation, we derive the improved Forchheimer equation that accounts for the combined effects of fracture surface roughness and temperature on the flow behavior of fractured rocks:

$$-\nabla P = \frac{12\mu}{we_h^3\eta^3}Q + \frac{\beta\rho(1+\omega)^{4/3}}{w^2\mathrm{JRC}^5(1-\omega)^{4/3}}Q^2 = AQ + BQ^2 \tag{9}$$

3. Experimental materials and method

3.1. Specimen preparation and measurement of fracture roughness

The carbonate rock specimens used in this experimental study were collected from the Tarim Basin, China. Each specimen was processed into a standard cylindrical shape with a diameter of 25 mm and a length of 50 mm. The average density of the specimens was 2.706 g/cm^3, and the uniaxial compressive strength was 73.5 MPa. Permeability tests were conducted on intact carbonate rock specimens, as shown in Fig. 3a, which exhibited a permeability of less than 10^{-20} m^2. The permeability of the rock matrix was considered negligible compared to that of the fractures. The Brazilian splitting test was conducted along the axial direction of the carbonate rock specimens, generating specimens with a single fracture (Fig. 3b).

Prior to seepage experiments, a high-precision 3D scanner was employed to capture the fracture surfaces morphology and acquire point cloud data. The point cloud data were imported into Geomagic Design X software for coordinate alignment and noise reduction. Subsequently, the data were imported into MATLAB for fracture surfaces reconstruction, as illustrated in Fig. 3c. The longer side of the fracture surface was considered the y-axis, the shorter side as the x-axis, and the direction of surface fluctuation as the z-axis. Each fracture surface was sampled at 100 points along the x-axis and 200 points along the y-axis. Based on various measurement methods, studies have derived a three-dimensional JRC calculation formula, which follows the JRC approach proposed by Barton, as expressed in the following equation [10]:

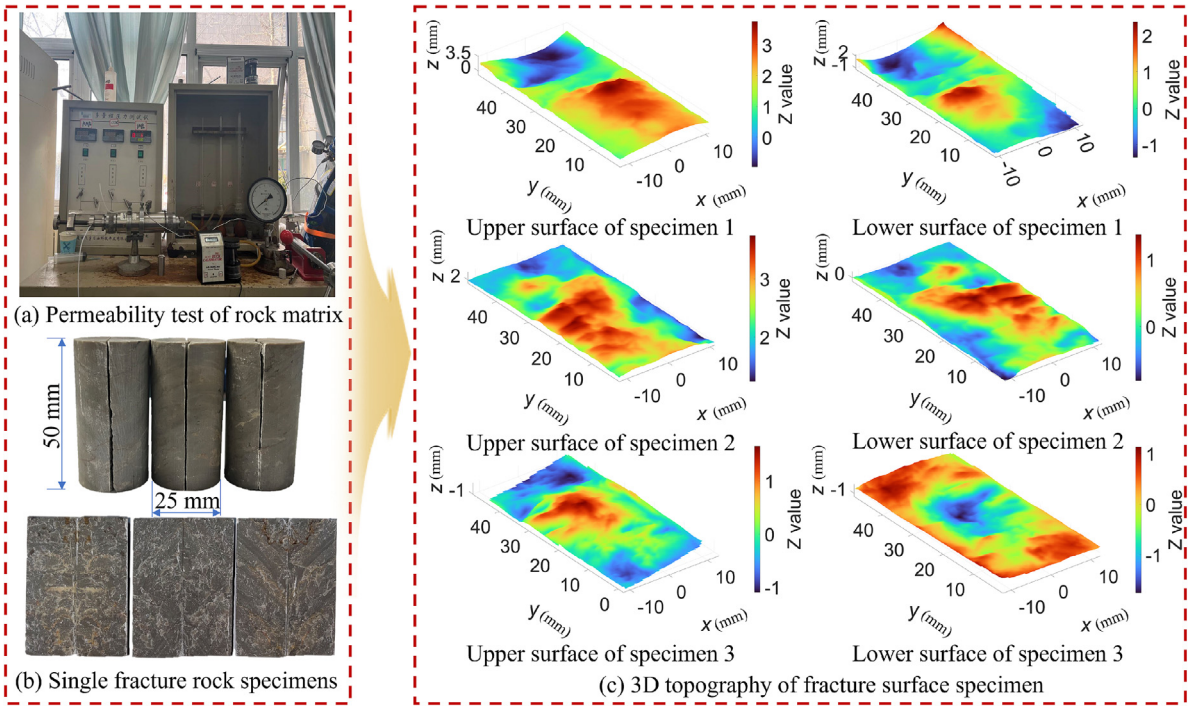

Fig. 3. Preparation before the seepage experiment on the rock with a single fracture.

$$z = \left\{ \left[\frac{1}{\Delta x^2} \sum_{i=1}^{N_x-1} \sum_{j=1}^{N_y-1} \frac{\left(Z_{i+1,j+1}-Z_{ij}\right)^2+\left(Z_{i+1,j}-Z_{i,j+1}\right)^2}{2} + \frac{1}{\Delta y^2} \sum_{j=1}^{N_x-1} \sum_{i=1}^{N_y-1} \frac{\left(Z_{i+1,j+1}-Z_{i+1,j}\right)^2+\left(Z_{i,j+1}-Z_{ij}\right)^2}{2} \right] / \left[(N_x-1)(N_y-1)\right] \right\}^{\frac{1}{2}} \tag{10}$$

$$\mathrm{JRC} = 32.2 + 32.47 \lg Z \tag{11}$$

where Z represents the dimensionless roughness parameter, and N_x and N_y the number of sampling points along the x-axis and y-axis, respectively. The intervals between sampling points along the x-axis and y-axis are denoted by Δx and Δy. z_i and z_{i+1} correspond to the z-axis coordinates of the i-th and (i+1)-th sampling points. The indices i and j represent the serial numbers of sampling points along the x and y directions, respectively.

3.2. Testing procedure

This study aims to reveal the evolution of fluid flow behavior in a single rock fracture under varying reservoir depths. A self-developed multi-field coupling test system was used to conduct seepage experiments, as shown in Fig. 4. Seepage experiments were conducted on single-fractured carbonate rock specimens with different roughness, under different temperatures, confining pressures, and seepage pressures. To avoid errors induced by fluid phase transitions, the experimental temperatures were selected at 20, 50, and 90 °C. The confining pressures were selected based on the classification of oil and gas reservoir depths in China, assuming a geostress gradient of 20 MPa/km: shallow reservoirs at 30 MPa (1500 m), intermediate reservoirs at 60 MPa (3000 m), deep reservoirs at 90 MPa (4500 m), and ultra-deep reservoirs at 120 MPa (above 6000 m). The maximum seepage pressures corresponding to these confining pressures were set at 15, 30, 45, and 60 MPa, respectively. The seepage pressure was applied in increments of 5 MPa until fluid flow stabilized, after which a higher pressure was applied until the target seepage pressure was reached.

To ensure that fluid flows exclusively along the fracture within the specimen, it is first immersed in a vacuum chamber filled with distilled water until no bubbles appear, indicating complete saturation. Next, a waterproof epoxy resin is uniformly applied along the circumferential direction of the fractured rock to ensure fluid flow along the fracture. Finally, rubber heat-shrinkable sleeves are used to seal the specimen along with the upper and lower porous plates, ensuring the integrity of the fluid flow path.

The specific steps for the seepage test are as follows:

(1) Experiment at 20 °C: The confining pressure was increased to 30 MPa and maintained at a stable level, after which the seepage pressure was applied. The seepage pressure was set at three levels: 5, 10, and 15 MPa. The pressure difference between the inlet and outlet of the specimen was continuously monitored using a differential pressure sensor. Once the flow stabilized under a constant seepage pressure, a precision electronic balance with an accuracy of 0.001 g was used to record the flow rate.
(2) The confining pressure was reduced to 0 MPa, after which the specimen was reinstalled. The confining pressure was then increased to 60 MPa, followed by the application of the seepage pressure. The seepage pressure was applied in increments of 5 MPa, ranging from 5 to 30 MPa. After each applied pressure, sufficient time was allowed for the flow rate to stabilize before recording the flow rate.
(3) Step (2) was repeated to conduct seepage experiments at target confining pressures of 90 and 120 MPa, with corresponding seepage pressure ranges of 5-45 MPa and 5–60 MPa, respectively.
(4) Seepage tests were conducted on the same specimen at 50 and 90 °C following the procedures outlined in steps (1)–(4). Note that the temperature must be kept for at least 8 h after reaching the target temperature to ensure thermal equilibrium throughout the experimental setup.

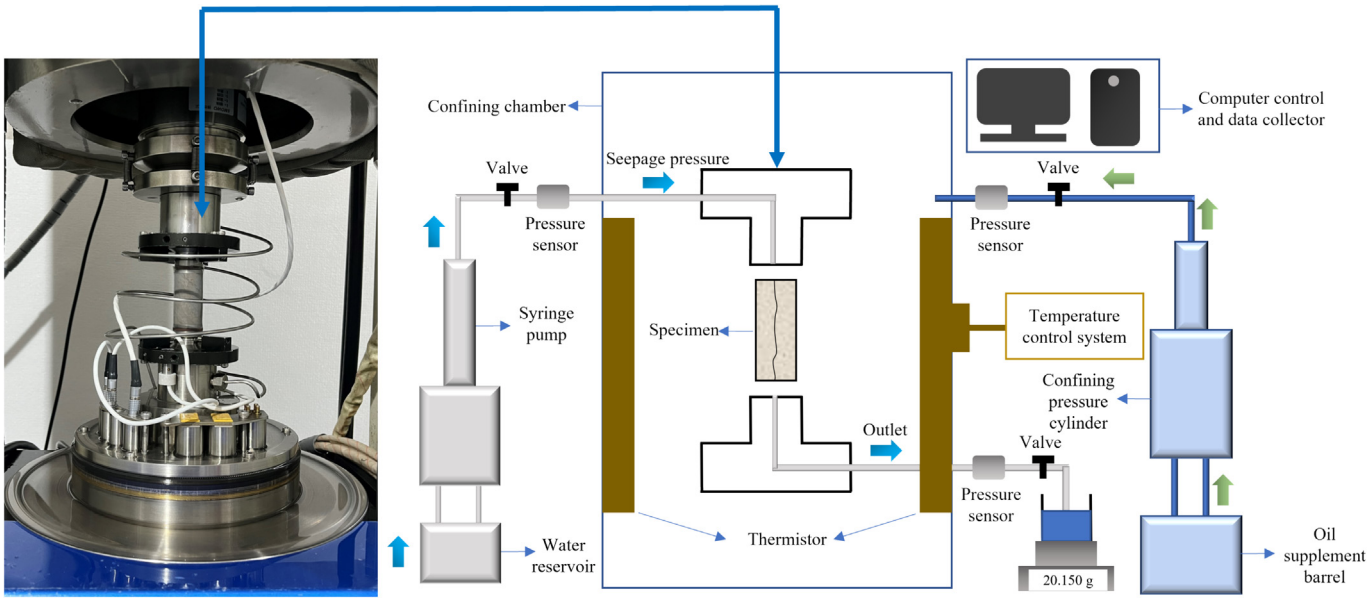

Fig. 4. Principle diagram of the seepage experiment system.

The experimental scheme effectively investigates the flow behavior of fractured specimens with different roughness under varying temperatures, confining pressures, and seepage pressures. In this study, fluid flow is assumed to occur exclusively along the fracture, while the permeability of the rock matrix is considered negligible. Experimental results validate this assumption, as the permeability of the fracture is more than six orders of magnitude higher than that of the rock matrix, even at a confining pressure of 120 MPa. Additionally, the erosion effect of the fluid on the fracture is neglected, and the roughness of the rock is assumed to remain unchanged throughout the experiment.

4. Experimental results

4.1. Effect of confining pressure on flow behavior of fractured rock

Fig. 5 presents the $-\nabla P$–Q curves for three rock specimens, each containing a single fracture with different roughness, under varying confining pressures at 20 °C. The curves were fitted using the Forchheimer equation, with correlation coefficients exceeding 0.99, indicating that the Forchheimer equation effectively describes the nonlinear relationship between volumetric flow rate and hydraulic gradient in fractured rocks under different confining pressures. The experimental results reveal that the linear term coefficient a in the Forchheimer equation increases with confining pressure, while the nonlinear term coefficient b exhibits different trends. Specifically, as the confining pressure increases from 30 to 60 MPa, the b value transitions from positive to negative. When the confining pressure exceeds 60 MPa, the b value decreases with increasing confining pressure. During the process of increasing the confining pressure from 30 to 120 MPa, the coefficient a increases by four orders of magnitude, and the absolute value of b changes by seven orders of magnitude. A similar phenomenon was also reported by Yu et al. [43].

It can be observed from Fig. 5 that a linear relationship exists between the volumetric flow rate and hydraulic gradient under the relatively low hydraulic gradient for each confining pressure. However, as the hydraulic gradient increases, two distinct nonlinear flow behaviors emerge. At a confining pressure of 30 MPa, the $-\nabla P$–Q curves exhibit an inward concave shape, whereas for confining pressures exceeding 60 MPa, the curves display an outward convex trend. This phenomenon can be attributed to different dominant mechanisms at varying confining pressures. At lower confining pressures (30 MPa), higher flow velocities induce inertial effects, leading to a more significant increase in the pressure gradient compared to the volumetric flow rate, thereby resulting in non-Darcy flow behavior. The convex nonlinear effect observed at confining pressures higher than 60 MPa is mainly attributed to strong fluid-solid coupling effects. The higher confining pressure reduces the hydraulic aperture, leading to low-velocity nonlinear flow behavior in rough rock fractures.

The variation in hydraulic aperture under different confining pressures is calculated and presented in Fig. 6a. At a given hydraulic gradient of 300 MPa/m (seepage pressure is 15 MPa), when the confining pressure is 30 MPa, the hydraulic aperture of the three specimens with different roughness is in the micrometer range. As the confining pressure rises to 60 MPa, the hydraulic aperture of single fracture rocks decreases by one order of magnitude. With a further increase in confining pressure, the rate of decrease in hydraulic aperture slows significantly. For Specimen 1, the hydraulic apertures at confining pressures of 30, 60, 90, and 120 MPa are 2.528, 0.457, 0.2402, and 0.161 μm, respectively. All specimens with different roughness follow a similar trend.

The effect of seepage pressure on the hydraulic aperture is shown in Fig. 6b. The hydraulic aperture increases with the hydraulic gradient, but the rate of increase gradually decreases as the confining pressure increases. Taking specimen 1 as an example, under a hydraulic gradient of 100 MPa/m (seepage pressure is 5 MPa), the hydraulic apertures at confining pressures of 30, 60, 90, and 120 MPa are 2.394, 0.444, 0.237, and 0.158 μm, respectively. When the hydraulic gradient increases to 300 MPa/m (seepage pressure is 15 MPa), the hydraulic aperture increases to 2.687, 0.453, 0.238, and 0.159 μm under different confining pressure conditions, with increases of 12.2%, 2.0%, 0.4%, and 0.6%, respectively. The results indicate that the effect of hydraulic gradient on the hydraulic aperture is significant under low to moderate confining pressures (≤60 MPa). When the confining pressure exceeds 90 MPa, the influence of seepage pressure on the hydraulic aperture diminishes.

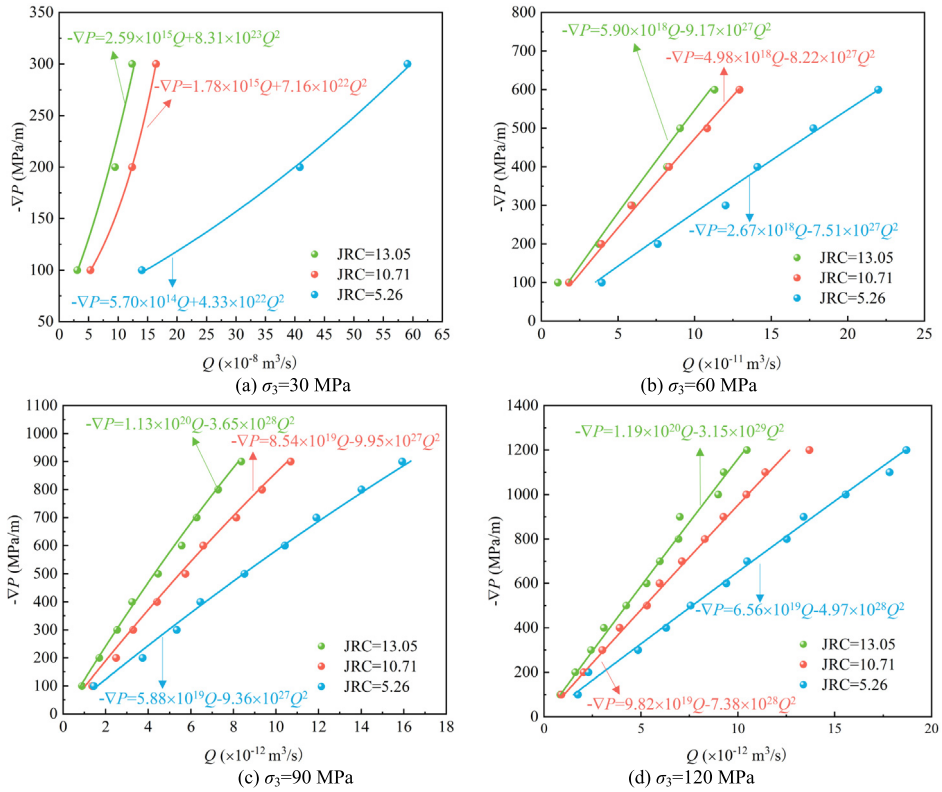

Fig. 5. The relationship between the hydraulic gradient ($-\nabla P$) and the volumetric flow rate (Q) of the specimens under different confining pressures at 20 °C.

The above analysis indicates that under different confining pressure conditions, applying the same seepage pressure results in varying deformation responses of the hydraulic aperture. To better characterize the influence of seepage pressure on hydraulic aperture under different confining pressures, we introduce the concept of relative seepage pressure, defined as the ratio of seepage pressure to confining pressure. Fig. 7 illustrates the influence of relative seepage pressure changes (ranging from 16.6% to 50%) on the hydraulic aperture of Specimen 1 (JRC=13.05) under different confining pressures. It can be observed that under low and medium confining pressures (≤60 MPa), increasing relative seepage pressure significantly enhances the hydraulic aperture. Specifically, when the confining pressure is 30 MPa, the relative seepage pressure increases from 16.6% to 33.3% and 50%, and the hydraulic aperture increases by 4.51% and 7.36%, respectively. However, under high confining pressure conditions (≥90 MPa), increasing the relative seepage pressure from 16.6% to 33.3% and 50% results in hydraulic aperture increases of less than 1.5%. This trend indicates that in ultra-deep reservoir environments, the influence of seepage pressure on fracture aperture is strongly constrained by confining pressure.

4.2. Effect of temperature on flow behavior of fractured rock

Fig. 8 shows the $-\nabla P$–Q curves of Specimen 1 (JRC=13.05) under different confining pressures and temperatures. The results show that the temperature does not alter the nonlinear flow pattern of fractured rock. Under the same confining pressure, as temperature increases, the volumetric flow rate under the same hydraulic gradient exhibits an increasing trend. This phenomenon is attributed to the decrease in fluid viscosity with increasing temperature, which reduces fluid flow resistance and enhances fluid mobility. As a result, larger flow rates can be achieved with a lower hydraulic gradient. In addition, the results fitted using the Forchheimer equation show that the coefficient a decreases with increasing temperature, whereas the coefficient b decreases with increasing temperature at lower confining pressures (≤30 MPa), but increases with the increase in temperature at higher confining pressures (≥60 MPa). This change is due to the fact that the coefficient a is related to the viscous resistance of the fluid. When the temperature increases, the viscosity of the fluid decreases, resulting in a reduction in a. The coefficient b in the Forchheimer equation reflects the nonlinear flow characteristics. Under low confining pressures, the fracture channel is not completely closed, and the inertial effect of the fluid is obvious. As the temperature increases, the inertial resistance decreases, resulting in a reduction in b. Under high confining pressures, the fracture aperture further closes, weakening the inertial effect of the fluid. This results in a decrease in the absolute value of b and a reduction in the nonlinear effect.

4.3. Effect of roughness on seepage characteristics of fractured rockz

Fig. 9 shows the variation of volumetric flow rate of fractured rock with JRC under different confining pressures (30, 60, 90, and 120 MPa) at a hydraulic gradient of 300 MPa/m. The results indicate that the fluid flow decreases with increasing JRC under the same hydraulic gradient. Specifically, when the confining pressure is 30 MPa, the volumetric flow rates of three single fracture rock specimens (with JRC values of 5.26, 10.71, and 13.05) are 5.91×10^{-7}, 1.64×10^{-7}, and 1.23×10^{-7} m^3/s, respectively. The volumetric flow rates of Specimen 1 and Specimen 2 are reduced by 79.2% and 72.2%, respectively, compared to Specimen 3. When the confining pressure increases to 60 MPa, the volumetric flow rate of single fractured rocks with different roughness decreases by one order of magnitude, which are 12.02×10^{-8}, 6.36×10^{-8}, 5.93×10^{-8} m^3/s, respectively, decreasing by 47.1% and 50.7%. As the confining pressure increases to 90 MPa, the volumetric flow

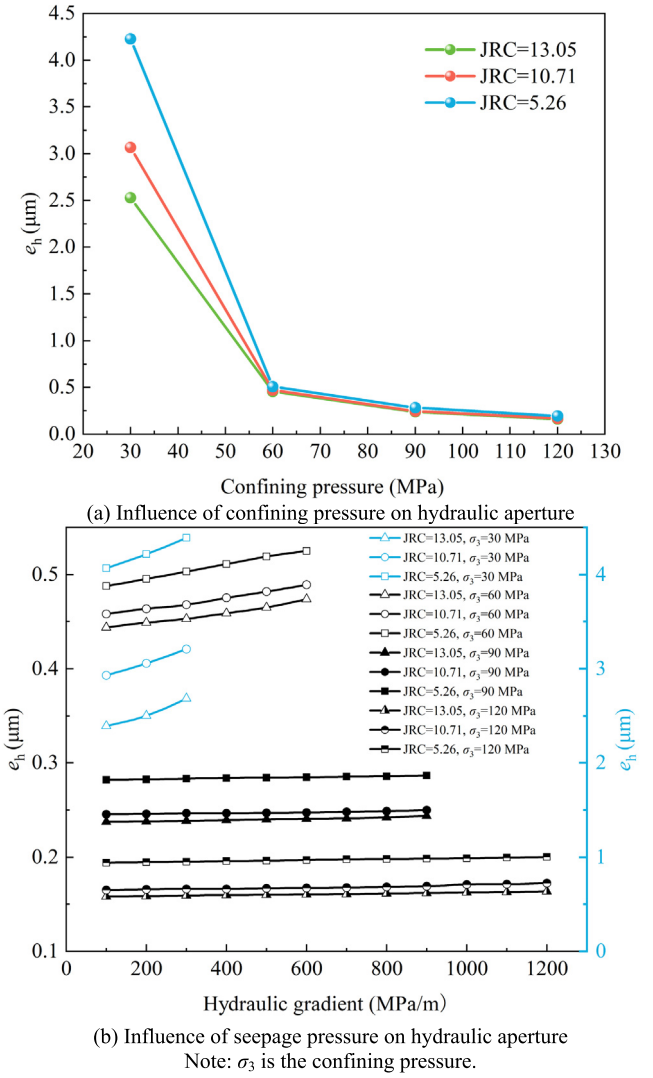

Fig. 6. Influence of confining pressure and hydraulic pressure on hydraulic aperture. Note: σ_3 is the confining pressure.

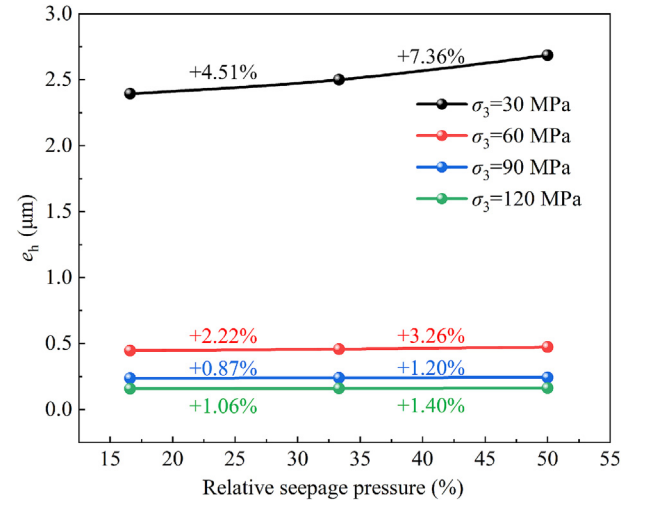

Fig. 7. Variation of hydraulic aperture with relative seepage pressure under different confining pressures.

rate continues to decrease with increasing JRC, with values of 5.34×10^{-12}, 3.29×10^{-12}, and 2.84×10^{-12} m^3/s, which decrease by 38.4% and 46.8%, respectively. These results indicate that under low confining pressures, the flow behavior of fractured rocks is significantly influenced by roughness. However, as the confining pressure increases, the impact of roughness on fluid flow diminishes.

In addition, it can be observed from Fig. 5 that the absolute values of *a* and *b* in the Forchheimer equation increase with increasing JRC. This phenomenon can be explained by the physical significance of *a* and *b* in the Forchheimer equation. The coefficient *a* represents the linear response of flow. As the roughness increases, the irregularity of the fracture surface becomes more pronounced, leading to increased frictional resistance during fluid flow. This increased resistance requires higher hydraulic pressure to overcome the surface friction, thus necessitating a larger value of *a*. The coefficient *b* is related to the nonlinear behavior of fluid flow. As the roughness of the fracture increases, the fluid flow path becomes more irregular and tortuous, promoting local flow instability and increasing the inertial effects, which increases the absolute value of *b*.

4.4. The effect of HTHM coupling on fluid flow behavior

Fig. 10 shows the $-\nabla P$–Q curves of single fractured rock with different roughness under various confining pressure and temperature conditions. The Forchheimer equation fitted under different working conditions is shown in Table 2. Under the same hydraulic gradient, as temperature increases and fracture surface roughness decreases, the volumetric flow rate of fractured rock increases. However, under different confining pressure conditions, the influence of temperature and roughness on the flow behavior of a single fractured rock changes. The flow behavior of rough rock fractures under HTHM conditions exhibits complex variations. To further explore the evolution of fluid flow under HTHM coupling, we plotted the volumetric flow rate of fractured rocks with different roughness as it varies with temperature and JRC under a hydraulic gradient of 200 MPa/m, as shown in Fig. 11.

By comparing the data in Fig. 11a-d, it can be observed that the effect of fracture roughness on volumetric flow rate decreases as the confining pressure increases. When the confining pressure is 30 MPa and the temperatures are 20, 50, and 90 °C, respectively, the volumetric flow rate increases by 229.46%, 230.27%, and 216.69% when the JRC of the fractured rock decreases from 10.71 to 5.26. However, when the confining pressure increases to 60 MPa, the increase in volumetric flow rate due to the same reduction in JRC significantly drops to 94.12%, 77.41%, and 87.82% at temperatures of 20, 50, and 90 °C, respectively.

The effect of temperature on the volumetric flow rate of fractured rock decreases with the increase in confining pressure, and this trend is more pronounced when the JRC of the fractured rock is higher. At a confining pressure of 30 MPa, when the temperature increases from 20 to 50 ℃ and 50 to 90 °C, the volumetric flow rate of Specimen 1 (JRC=13.05) increases by 44.06% and 24.41%, respectively. However, when the confining pressure increases to 90 MPa, the corresponding increments reduce to 36.79% and 16.69%, and further decrease to 24.41% and 11.61% at 120 MPa. Similar trends are observed in Specimens 2 and 3. This is because, after the confining pressure reaches a certain value (≥90 MPa), the hydraulic aperture significantly decreases and tends to stabilize. Even though an increase in temperature can reduce the fluid viscosity and decrease flow resistance, the extremely narrow hydraulic aperture significantly limits the flow path of the fluid, indicating that the viscosity changes caused by temperature cannot effectively improve the fluid flow in the fracture.

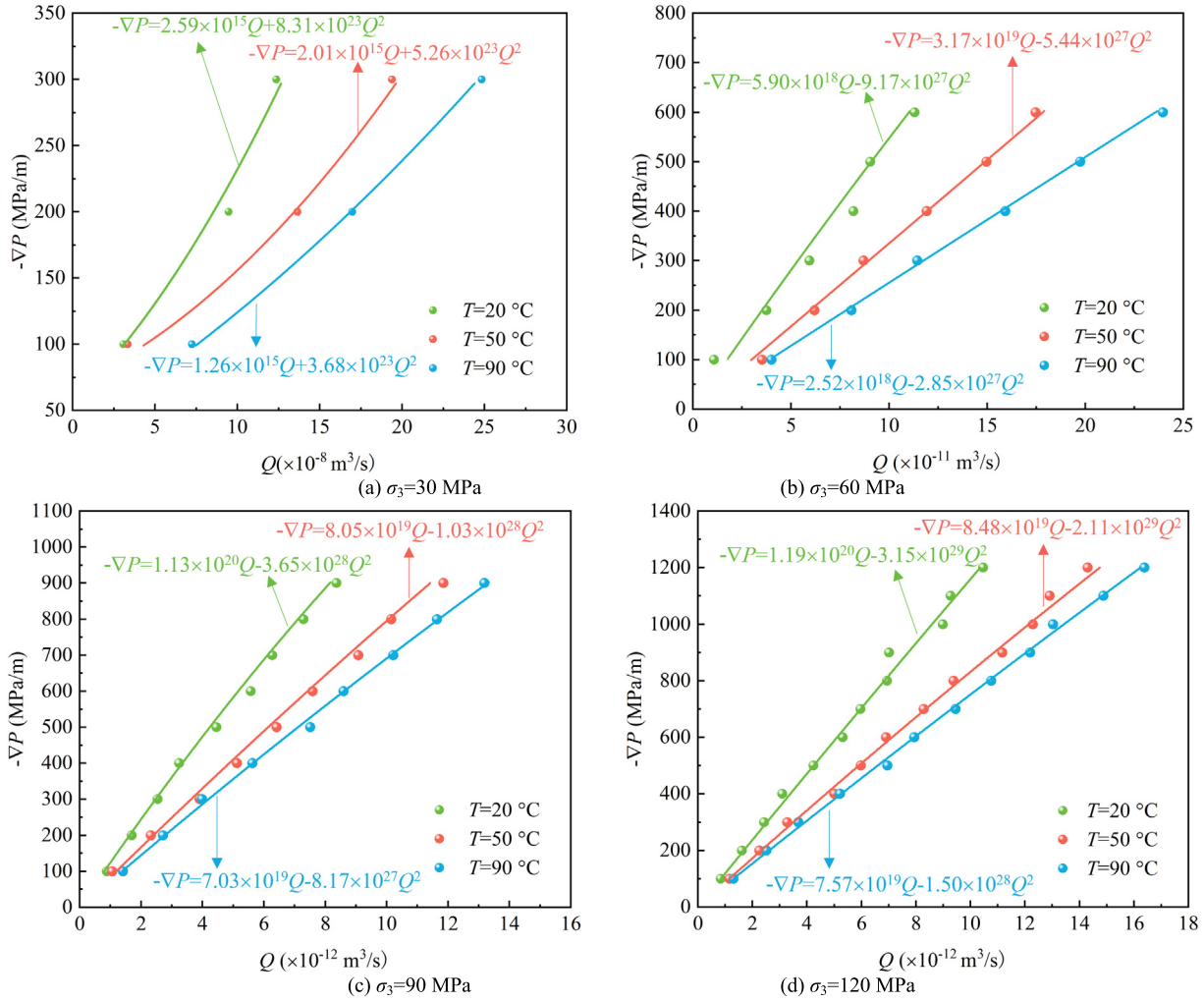

Fig. 8. Relationship between the hydraulic gradient ($-\nabla P$) and the volumetric flow rate (Q) of Specimen 1 at different temperatures.

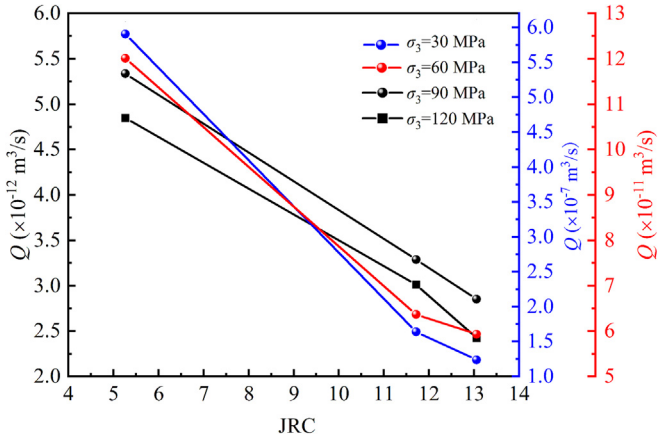

Fig. 9. The volumetric flow rate varies with JRC when the hydraulic gradient is 300 MPa/m.

The effects of temperature and roughness on the flow behavior of a single rock fracture vary with confining pressure. At a confining pressure of 30 MPa, the influence of temperature on the volumetric flow rate of fractured rocks becomes more pronounced as roughness decreases. When the temperature increases from 20 to 50 °C the volumetric flow rate of Specimens 1, 2, and 3 (with JRC values of 13.05, 10.71, and 5.26, respectively) increases by 44.06%, 49.39%, and 49.77%, while the volumetric flow rate increases by 24.41%, 27.93%, and 33.23%, respectively, as the temperature rises from 50 to 90 °C At this confining pressure, the influence of roughness on the volumetric flow rate of fractured rocks is not significantly affected by temperature. At lower confining pressures, when the JRC of fractured rocks ranges from 10.71 to 5.26 and the temperature varies between 20 and 90 °C, the influence of roughness on volumetric flow rate is clearly greater than the effect of temperature. However, as confining pressure increases, the influence of roughness on the flow behavior of fractured rocks diminishes as the hydraulic aperture decreases, while the influence of temperature on volumetric flow rate remains relatively stable. In general, the influence of temperature and roughness on flow behavior is constrained by confining pressure. As confining pressure increases, the reduction in hydraulic aperture and the limitation of fluid flow paths cause the impact of these factors on volumetric flow rate to gradually diminish. The combined influence of roughness and temperature on volumetric flow rate is significant under low confining pressure (≤30 MPa), whereas at high confining pressure, the effect of temperature stabilizes, and the influence of roughness gradually diminishes.

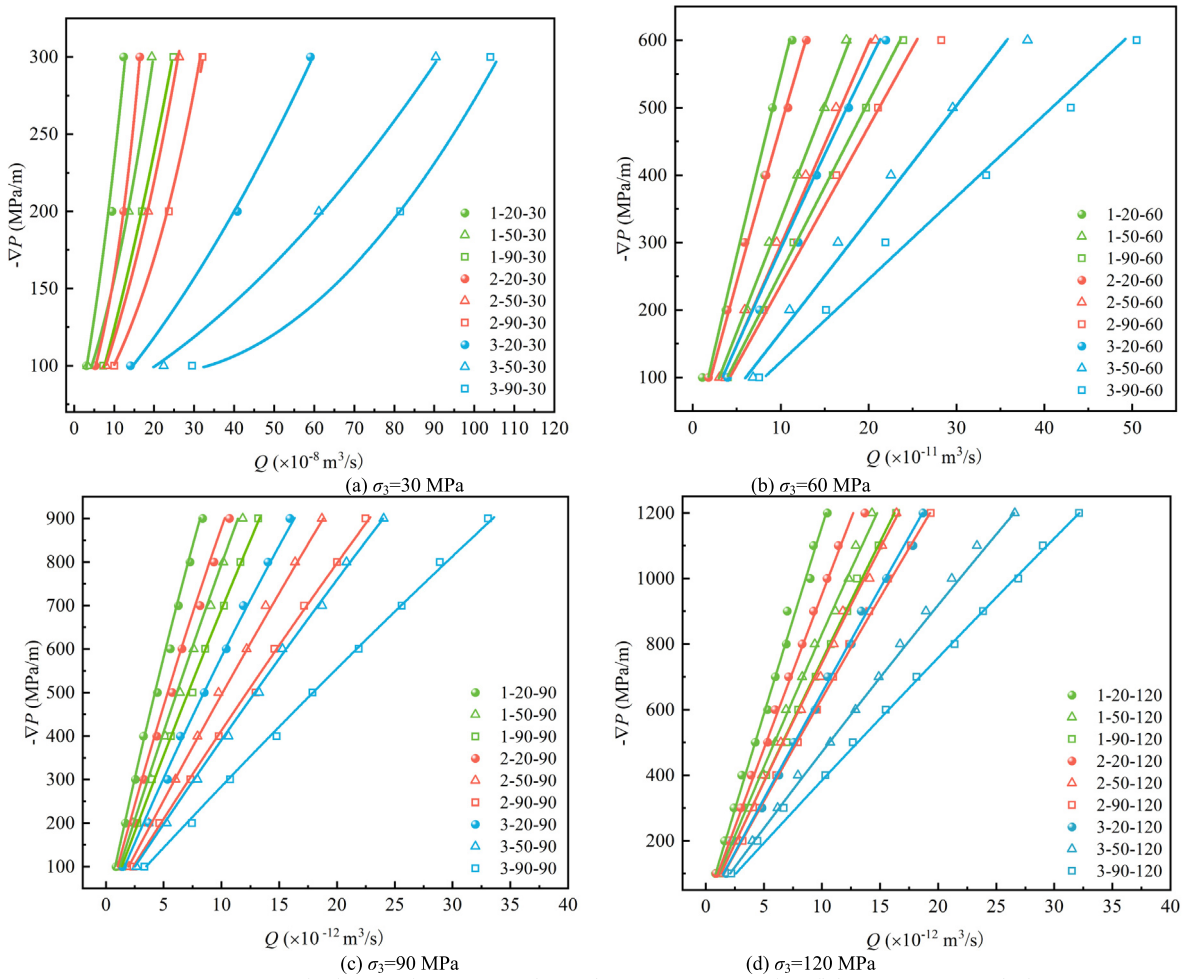

Note: 1–20–90, the three numbers represent the specimen, temperature, and confining pressure, respectively.

Fig. 10. Relationship between the hydraulic gradient ($-\nabla P$) and the volumetric flow rate (Q) of the three specimens with a single rough fracture at different temperatures and confining pressures.

5. Discussion

5.1. Applicability of the improved Forchheimer equation

To verify the accuracy of the improved Forchheimer equation in describing the behavior of fluid in fractured rock, it is essential to first calculate the contact ratio of the fracture surface. Given the complexity of the experimental setup in this study, the contact area ratio was determined through the following procedure.

Step 1: Using the point cloud data of the upper and lower fracture surfaces obtained from a 3D scanner, the fracture surfaces were geometrically aligned and stitched based on the spatial registration method described in Section 3.1.

Step 2: The local aperture at each point on the fracture surface was calculated. Specifically, we selected a grid of 100 points along the x-axis and 200 points along the y-axis to represent the surface morphology. The aperture distribution was then computed along different x-coordinates across the fracture plane.

$$e_I^0 = Z_I^0 - z_I^0 \tag{12}$$

where e_I^0 denotes the natural (unloaded) aperture at each data point within the fracture surface; I the index of the data point; Z_I^0 and z_I^0 the z-axis coordinates of the corresponding points on the upper and lower fracture surfaces, respectively.

Step 3: The aperture of fractured rock after external load is calculated as follows:

$$e_I = e_I^0 - \Delta e \tag{13}$$

where e_I is the aperture at each data point within the fracture; and Δe the fracture aperture variation. In this study, the aperture variation at each data point on the fracture surface after the experiment was recalculated, with the difference between the corresponding data points before and after loading defined as Δe.

Step 4: The contact area ratio can be expressed:

$$\omega = \frac{\sum_{I=1}^{N_t} S_I}{S_a} = \frac{\sum_{I=1}^{N_t} b_I}{N_t} \tag{14}$$

where S_I is the area of corresponding unit data points on the upper and lower fracture contact surfaces; S_a the total area in a fracture surface; b_I the contact ratio coefficient of data points in the fracture surface; and N_t the total number of data points on a fracture surface. When e_I is less than or equal to 0.0005 mm, the value of b_I is 1, and when e_I is greater than 0.0005 mm, the value of b_I is 0.

Fig. 12 presents the natural and stress-induced fracture apertures along the y-axis at five representative positions (x=−10, −5, 0, 5, and 10 mm) for Specimens 1, 2, and 3. Specifically, Fig. 13a and b illustrate the natural (unloaded) aperture and stress-induced aperture distribution. Based on Eqs. (12)–(14), the

Table 2
Summary of Forchheimer equations under different conditions.

Confining pressure (MPa)	Specimen	Temperature (°C)	Equation	Confining pressure (MPa)	Specimen	Temperature (°C)	Equation
30	1	20	$-\nabla P = 2.59 \times 10^{15}Q + 8.31 \times 10^{23}Q^2$	60	1	20	$-\nabla P = 5.90 \times 10^{18}Q - 9.17 \times 10^{27}Q^2$
		50	$-\nabla P = 2.01 \times 10^{15}Q + 5.26 \times 10^{23}Q^2$			50	$-\nabla P = 3.17 \times 10^{18}Q - 5.44 \times 10^{27}Q^2$
		90	$-\nabla P = 1.26 \times 10^{15}Q + 2.78 \times 10^{23}Q^2$			90	$-\nabla P = 2.52 \times 10^{18}Q - 2.85 \times 10^{27}Q^2$
	2	20	$-\nabla P = 1.78 \times 10^{15}Q + 7.16 \times 10^{22}Q^2$		2	20	$-\nabla P = 6.85 \times 10^{18}Q - 8.22 \times 10^{27}Q^2$
		50	$-\nabla P = 1.16 \times 10^{15}Q + 4.56 \times 10^{22}Q^2$			50	$-\nabla P = 4.96 \times 10^{18}Q - 4.38 \times 10^{26}Q^2$
		90	$-\nabla P = 9.26 \times 10^{14}Q + 9.55 \times 10^{21}Q^2$			90	$-\nabla P = 2.46 \times 10^{18}Q - 1.82 \times 10^{27}Q^2$
	3	20	$-\nabla P = 5.70 \times 10^{14}Q + 4.33 \times 10^{22}Q^2$		3	20	$-\nabla P = 5.88 \times 10^{18}Q - 7.51 \times 10^{27}Q^2$
		50	$-\nabla P = 3.68 \times 10^{14}Q + 8.69 \times 10^{21}Q^2$			50	$-\nabla P = 3.79 \times 10^{18}Q - 5.27 \times 10^{27}Q^2$
		90	$-\nabla P = 2.91 \times 10^{14}Q + 1.54 \times 10^{22}Q^2$			90	$-\nabla P = 2.77 \times 10^{18}Q - 2.20 \times 10^{27}Q^2$
90	1	20	$-\nabla P = 1.13 \times 10^{20}Q - 3.65 \times 10^{28}Q^2$	120	1	20	$-\nabla P = 1.19 \times 10^{20}Q - 3.15 \times 10^{29}Q^2$
		50	$-\nabla P = 8.05 \times 10^{19}Q - 2.03 \times 10^{28}Q^2$			50	$-\nabla P = 8.48 \times 10^{19}Q - 2.11 \times 10^{29}Q^2$
		90	$-\nabla P = 7.03 \times 10^{19}Q - 8.17 \times 10^{27}Q^2$			90	$-\nabla P = 7.57 \times 10^{19}Q - 9.50 \times 10^{28}Q^2$
	2	20	$-\nabla P = 8.54 \times 10^{19}Q - 9.95 \times 10^{27}Q^2$		2	20	$-\nabla P = 9.82 \times 10^{19}Q - 7.38 \times 10^{28}Q^2$
		50	$-\nabla P = 5.03 \times 10^{19}Q - 7.68 \times 10^{27}Q^2$			50	$-\nabla P = 7.29 \times 10^{19}Q - 6.72 \times 10^{28}Q^2$
		90	$-\nabla P = 4.09 \times 10^{19}Q - 2.57 \times 10^{27}Q^2$			90	$-\nabla P = 6.31 \times 10^{19}Q - 2.33 \times 10^{28}Q^2$
	3	20	$-\nabla P = 5.88 \times 10^{19}Q - 9.36 \times 10^{27}Q^2$		3	20	$-\nabla P = 6.56 \times 10^{19}Q - 4.97 \times 10^{28}Q^2$
		50	$-\nabla P = 3.79 \times 10^{19}Q - 5.33 \times 10^{27}Q^2$			50	$-\nabla P = 4.81 \times 10^{19}Q - 3.82 \times 10^{28}Q^2$
		90	$-\nabla P = 2.77 \times 10^{19}Q - 4.50 \times 10^{27}Q^2$			90	$-\nabla P = 3.99 \times 10^{19}Q - 1.14 \times 10^{28}Q^2$

calculated contact area ratios for Specimens 1, 2, and 3 under 120 MPa are 0.67, 0.71, and 0.73, respectively. Chen et al. [44] systematically investigated the influence of fracture geometry on fluid flow behavior in fractured rocks and found that, with increasing confining pressure, the contact area ratio tends to increase initially and then stabilize. This stabilization becomes particularly evident when the confining pressure exceeds 20 MPa. Given that the confining pressures applied in this study range from 30 to 120 MPa, it is reasonable to assume that the contact area ratio remains relatively stable throughout this range. Therefore, the contact ratio calculated at 120 MPa was adopted as representative in the subsequent analysis.

Fig. 13 illustrates the effect of temperature on the density and dynamic viscosity coefficient of water. As the temperature increases from 20 to 50 and 90 °C, the dynamic viscosity decreases by 45.95% and 70.64%, respectively, and the density decreases by 0.99% and 3.29%, respectively.

Based on Eq. (10), the relationship between the hydraulic gradient and volumetric flow rate for specimens at different temperatures under a confining pressure of 30 MPa was determined, as shown in Fig. 14a. The results demonstrate that the improved Forchheimer equation effectively characterizes the flow behavior of single-fractured rocks under various environmental conditions. In this study, the thermal expansion coefficient is calculated based on calcite properties, $\frac{\alpha(T_{20})}{\alpha(T_{50})}$ and $\frac{\alpha(T_{20})}{\alpha(T_{90})}$ are 0.94 and 0.87, respectively [45]. Notably, under the same confining pressure, the β value shows a temperature dependence, which can be expressed as follows:

$$\beta = \beta_0 \frac{T}{T_0}\left(-0.804 + 1.3606 \times 0.995^{T}\right) \tag{15}$$

where β_0 is the modified Forchheimer equation parameter obtained from experiments at the reference temperature T_0; and T the predicted temperature.

Considering the temperature-dependent characteristics of the β value, the relationship between the hydraulic gradient and the volumetric flow rate of fractures with different roughness at 20 ℃ was first determined under confining pressures of 60, 90, and 120 MPa using Eq. (9). Subsequently, the relationship between the hydraulic gradient and the volumetric flow rate at 50 and 90 ℃ under the same confining pressures were predicted by Eqs. (9) and (15), as shown in Fig. 14ab–d. It is observed that, compared to the traditional Forchheimer equation, the modified Forchheimer equation proposed in this study effectively characterizes fluid flow behavior in rough fractures under complex conditions by incorporating parameters related to the rock thermal expansion coefficient, fracture surface roughness, and geometric characteristics. Furthermore, in the modified Forchheimer equation, parameters under high-temperature conditions can be derived from low-temperature experimental data, enabling the prediction of fluid flow behavior in rock fractures under higher temperatures.

Table 3 shows the fitting and predicted values of β for a single fracture with different roughness under different confining pressures. The corresponding β values at 50 and 90 ℃ are predicted values. It can be seen that Eq. (15) provides a good prediction of β under higher temperatures. In fact, under high-speed flow state, β in the Forchheimer equation serves as the nonlinear term coefficient, primarily characterizing the inertial effect in the fluid. The value of β is not only closely related to the structure and fracture roughness, as well as other external environmental factors, but also influenced by fluid properties, with density being the most direct variable in the Forchheimer equation. Under high-speed flow conditions, the inertial effect causes the fluid flow to deviate from Darcy's law [46]. In complex seepage paths or low-permeability media, the nonlinear term β demonstrates the sensitivity of fluid flow to the characteristics of complex media. In the above two cases, many researchers have investigated the determination of β through experimental methods, numerical simulations, and theoretical derivations. The results indicate that different factors, including material properties, fracture geometry, porosity, and size, all have an impact on β [47,48]. It is still a challenging problem to accurately describe the physical significance of β.

5.2. Sensitivity analysis of model parameters

To evaluate the influence of key parameters on fluid flow behavior, a sensitivity analysis of Eq. (9) was performed at a confining pressure of 30 MPa. During the sensitivity analysis, only

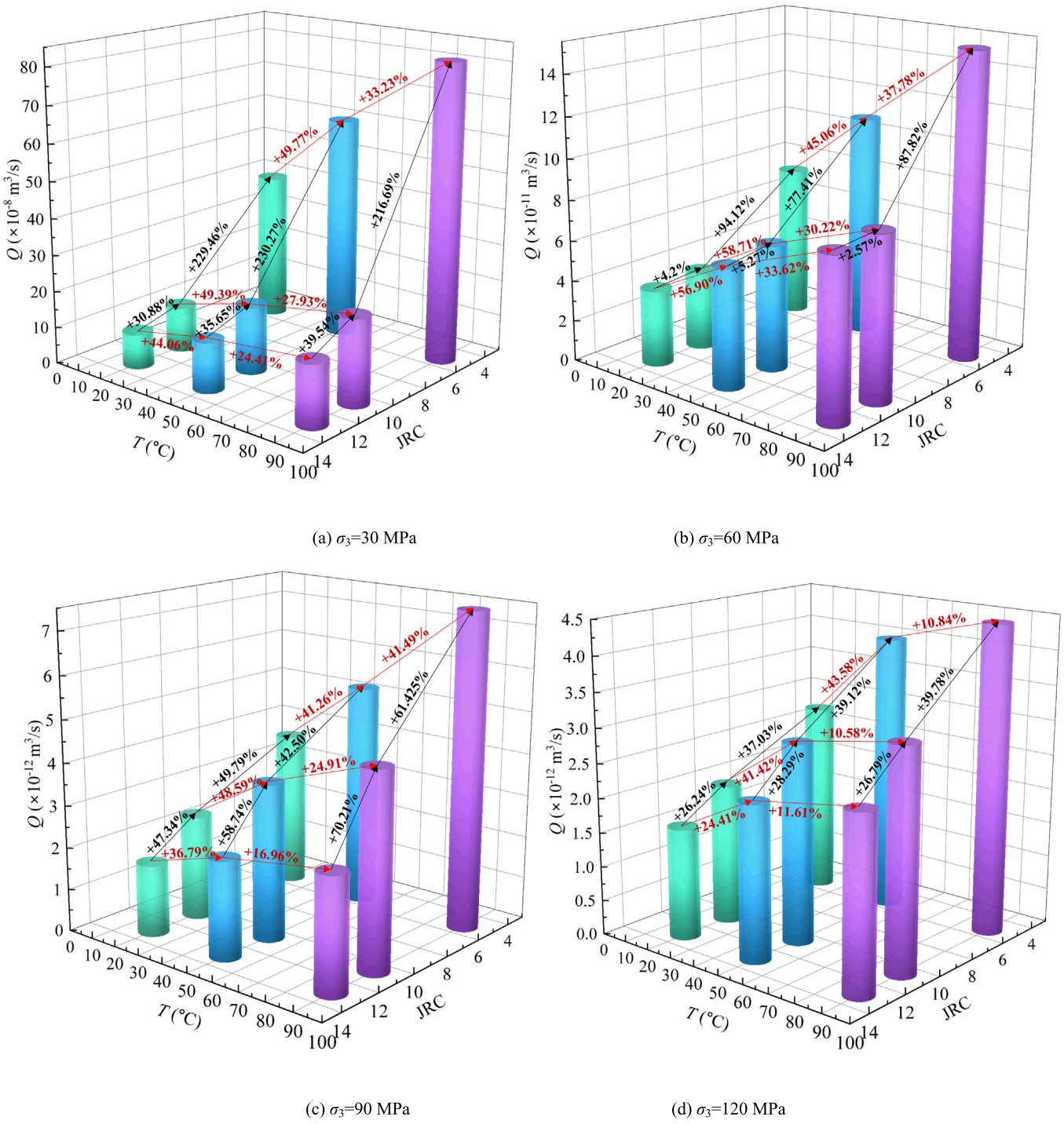

(a) σ_3=30 MPa

(b) σ_3=60 MPa

(c) σ_3=90 MPa

(d) σ_3=120 MPa

Fig. 11. Volumetric flow rate of different rough fractured rocks varies with temperature and JRC under the same hydraulic pressure.

the target parameter was varied, while all other parameters were held constant. Since temperature variations simultaneously affect the dynamic viscosity and density of the fluid, these two parameters were considered together as coupled factors in the analysis.

Fig. 15 illustrates the influence of fracture roughness parameters (JRC and ω) and temperature-related parameters (μ, ρ, and η) on flow behavior under a confining pressure of 30 MPa. The results, consistent with experimental findings, indicate that increasing JRC requires a larger pressure gradient to maintain the same volumetric flow rate, suggesting that increased roughness enhances flow resistance. A lower contact area ratio also leads to reduced volumetric flow rate under the same pressure gradient. In addition, as temperature increases, both fluid density and viscosity decrease, resulting in slightly lower flow resistance. As shown in Fig. 15c, when the temperature rises from 20 to 90 °C, the flow capacity increases only moderately. Notably, the thermal

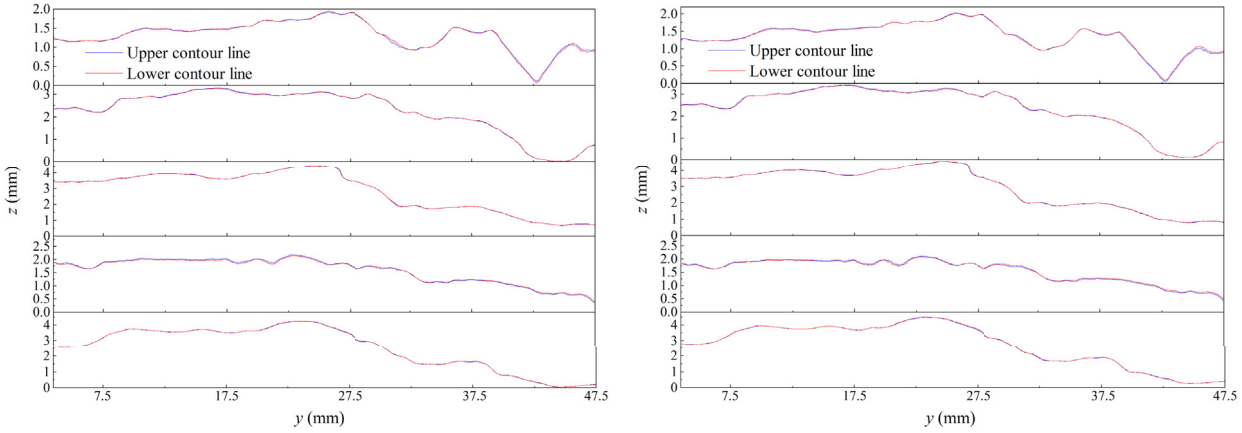

(a) Aperture distribution of Specimen 1 under σ_3=0 MPa (b) Aperture distribution of Specimen 1 under σ_3=120 MPa

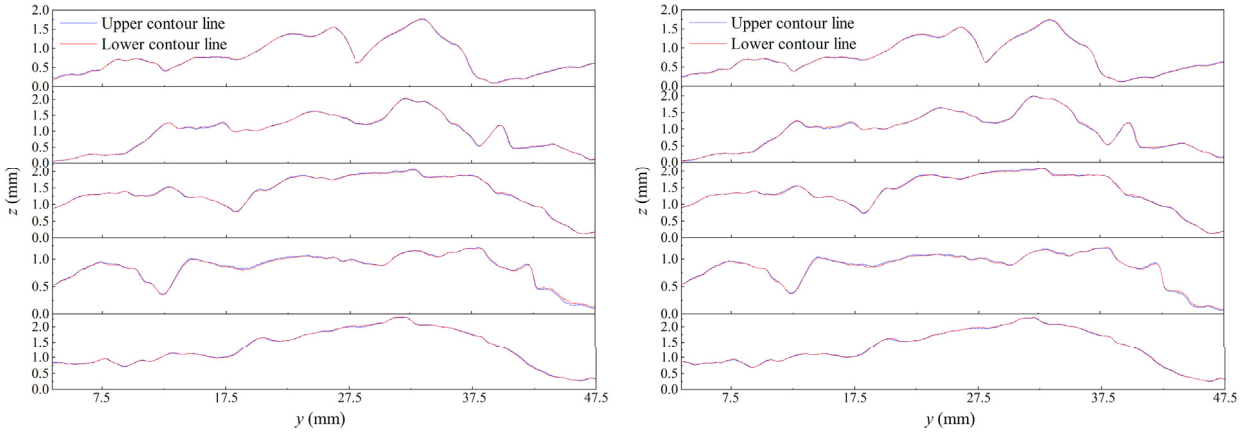

(c) Aperture distribution of Specimen 2 under σ_3=0 MPa (d) Aperture distribution of Specimen 2 under σ_3=120 MPa

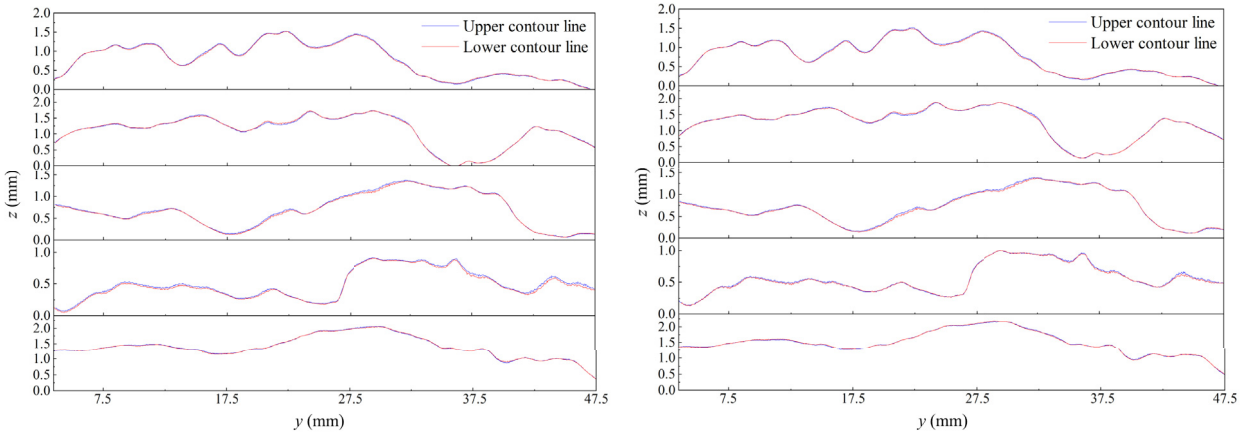

(e) Aperture distribution of Specimen 3 under σ_3=0 MPa (f) Aperture distribution of Specimen 3 under σ_3=120 MPa

Fig. 12. Aperture distribution of the specimens under natural and loaded conditions.

expansion coefficient ratio, introduced as a key parameter in the modified Forchheimer equation, plays a significant role in representing the thermo-hydro coupling. As temperature increases, this ratio decreases, indicating that thermally induced contraction of the hydraulic aperture occurs, which increases flow resistance. This parameter is crucial for characterizing the interaction between fluid flow and fracture deformation, and serves as a key factor for predicting flow behavior at elevated temperatures.

5.3. Transformation of linear-nonlinear flow behavior of a single rock fracture under THTM conditions

To quantify the degree of nonlinear fluid flow, two dimensionless parameters are commonly used: the Reynolds number (*Re*) and the non-Darcy effect factor F_0. The Reynolds number *Re* is defined as follows [49]:

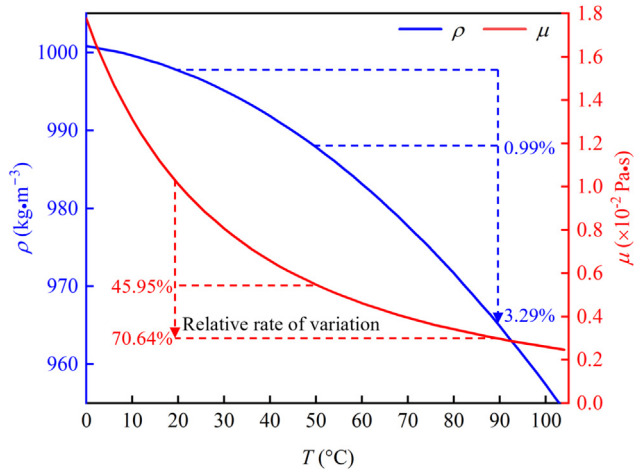

Fig. 13. Variation of density and dynamic viscosity coefficient of water with temperature.

$$Re = \frac{2\rho Q}{\mu w} \tag{16}$$

The larger the Reynolds number, the greater the inertia effect of the fluid. Previous literature has reported a wide range from 0.001 to 2300 of Reynolds number to distinguish between linear and nonlinear fluid flow regimes [42]. Due to the limited applied hydraulic gradients, studies have rarely focused on the nonlinear fluid flow behavior in naturally rough fractured rocks under high confining pressure and high hydraulic gradient conditions. Qian et al. [50] carried out experimental tests under high hydraulic gradients, and the Reynolds number *Re* varied from 2881 to 290338, which greatly exceeded the critical value of 2300.

The ratio of the hydraulic gradient caused by nonlinearity to the total hydraulic gradient is defined as the non-Darcy effect factor F_0. Generally, F_0=0.1 is considered the critical threshold for the transition from linear to nonlinear. When F_0>0.1, the flow exhibits non-Darcy behavior [23].

$$F_0 = \frac{bQ^2}{aQ + bQ^2} \tag{17}$$

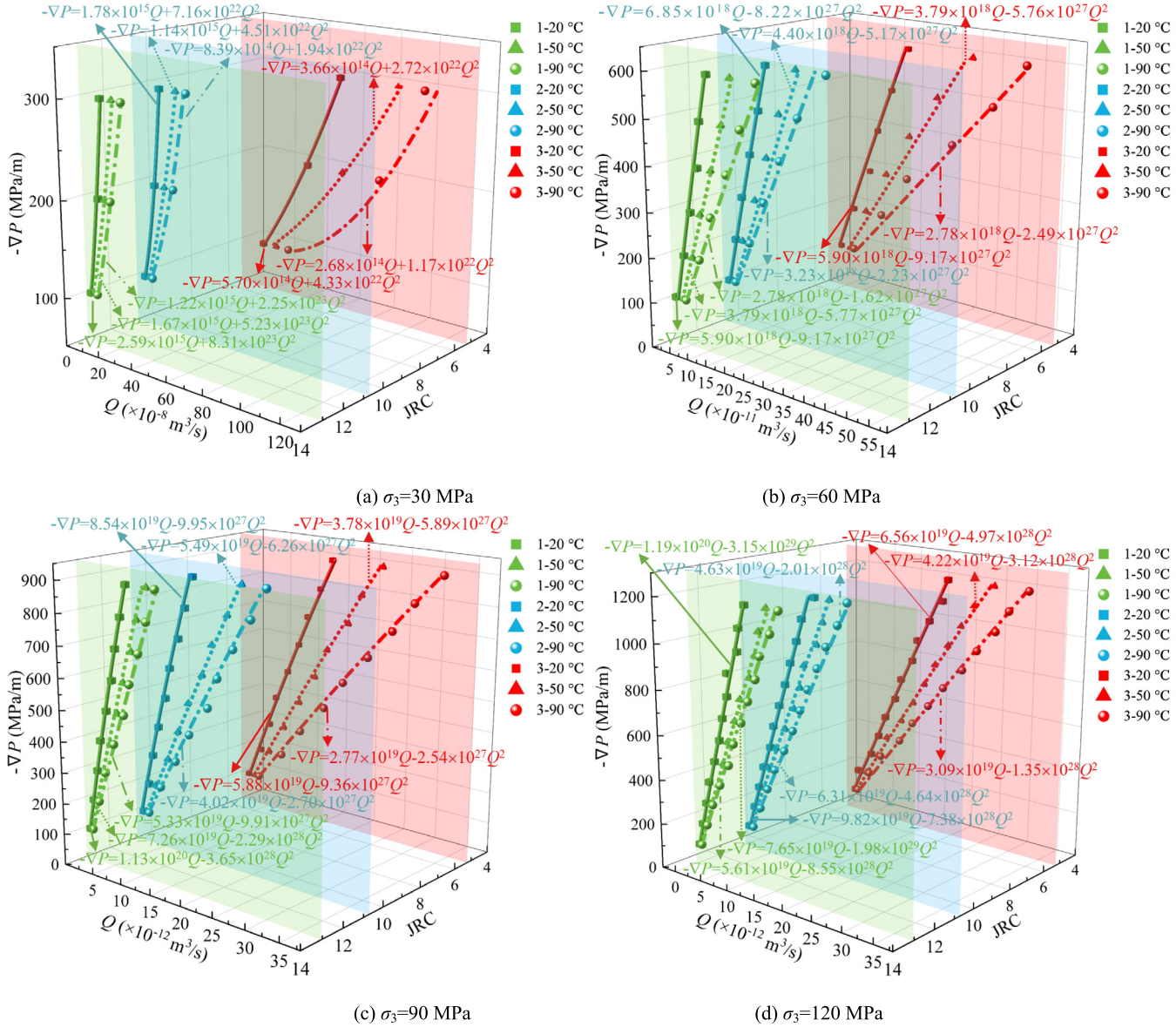

Fig. 14. Improved Forchheimer equation predicts the seepage behavior of fractured rock under high temperature.

Table 3
Comparison of β between fitting and predicted data.

Specimen	Confining pressure (MPa)	Temperature (°C)	Fitting value of β	Predicted value of β	Relative error (%)
1	30	50	1.471×10^{22}	1.442×10^{22}	2.052
		90	5.982×10^{21}	6.371×10^{21}	6.106
	60	50	-1.623×10^{26}	-1.591×10^{26}	2.006
		90	-4.741×10^{25}	-4.572×10^{25}	3.699
	90	50	-5.898×10^{26}	-6.334×10^{26}	6.888
		90	-2.706×10^{26}	-2.798×10^{26}	3.300
	120	50	-5.567×10^{27}	-5.466×10^{27}	1.841
		90	-2.675×10^{27}	-2.415×10^{27}	10.764
2	30	50	3.849×10^{20}	3.773×10^{20}	2.030
		90	1.722×10^{20}	1.666×10^{20}	3.319
	60	50	-4.418×10^{25}	-4.331×10^{25}	2.011
		90	-1.765×10^{25}	-1.913×10^{25}	7.765
	90	50	-4.929×10^{25}	-5.246×10^{25}	5.989
		90	-2.304×10^{25}	-2.316×10^{25}	0.499
	120	50	-3.966×10^{26}	-3.889×10^{26}	2.001
		90	-1.782×10^{26}	-1.718×10^{26}	3.730
3	30	50	5.951×10^{18}	5.836×10^{18}	1.962
		90	2.366×10^{18}	2.578×10^{18}	8.201
	60	50	-1.261×10^{24}	-1.236×10^{24}	2.007
		90	-5.084×10^{23}	-5.460×10^{23}	6.885
	90	50	-1.182×10^{24}	-1.261×10^{16}	6.342
		90	-5.084×10^{23}	-5.573×10^{23}	0.124
	120	50	-6.828×10^{24}	-6.699×10^{24}	1.933
		90	-2.958×10^{24}	-2.959×10^{24}	0.028

When the confining pressure increases to 60 MPa, it is difficult to change the Reynolds number significantly by increasing the seepage pressure due to the reduction in the hydraulic aperture caused by the elevated confining pressure. Fig. 16 illustrates the variation in the Reynolds number of a single rock fracture with temperature and roughness under different confining pressures at a hydraulic gradient of 200 MPa/m. It can be observed that the Reynolds number exhibits a positive correlation with temperature and a negative correlation with roughness under all four confining pressure levels. As the confining pressure increases from 30 to 60 MPa, the Reynolds number decreases by four orders of magnitude. When the confining pressure increases from 60 to 90 MPa, the Reynolds number decreases by one order of magnitude. Beyond 90 MPa, the effect of confining pressure on the Reynolds number gradually diminishes.

At a constant confining pressure, temperature, and roughness have a significant impact on the Reynolds number. When the confining pressure is 30 MPa and the temperature is 20 °C, the Reynolds numbers of Specimens 1, 2, and 3 are 6.64, 9.08, and 30.38, respectively. This means that when the JRC of a single fractured rock decreases from 13.05 to 5.26, the Reynolds number increases by 357.53%. When the temperature increases to 90 °C, the Reynolds numbers of the three fractured rocks become 41.02, 54.99, and 179.79, respectively. Compared to the values at 20 °C, the Reynolds numbers increase by 517.71%, 505.61%, and 491.80%, respectively. This means that when the JRC of a single rock fracture decreases from 13.05 to 5.26, the Reynolds number increases by 338.29%. These results demonstrate that an increase in temperature and a decrease in roughness lead to a higher Reynolds number. However, as confining pressure increases, the influence of temperature and roughness on the Reynolds number gradually diminishes. When the confining pressure is 90 MPa, and the temperature rises from 20 to 90 °C the Reynolds numbers of Specimens 1, 2, and 3 increase by 394.75%, 432.20%, and 446.63%, respectively. When the temperature is 20 and 90 °C, the roughness of a single fractured rock decreases from 13.05 to 5.26, and the Reynolds number increases by 192.77% and 285.87%, respectively.

To investigate the effects of confining pressure, seepage pressure, fracture surface roughness, and temperature on the nonlinear flow behavior of a single fractured rock, the non-Darcy effect factor (F_0) was calculated under different experimental conditions. At a low confining pressure of 30 MPa, the fracture aperture is at the micron level, resulting in significant nonlinear Forchheimer flow behavior when the fluid flows through the fracture. However, as the confining pressure increases to 90 MPa, the hydraulic aperture decreases to the sub-micrometer scale, with F_0 values consistently remaining below 0.1. Temperature and roughness exhibit minimal effects on the nonlinear flow behavior of fractured rock. Therefore, this study mainly discusses the effects of fracture roughness and temperature on nonlinear Forchheimer flow behavior under low (30 MPa) and medium confining pressures (60 MPa).

As shown in Fig. 17, an increase in both temperature and fracture roughness enhances the nonlinear Forchheimer flow behavior of a single rock fracture. Notably, the effects of temperature and roughness on the nonlinear flow behavior vary with different confining pressures. At a confining pressure of 30 MPa and a hydraulic gradient of 200 MPa/m, as the temperature increases from 20 to 90 °C, the F_0 value of Specimen 1 rises from 42.95% to 52.30%, while that of Specimen 3 increases from 63.87% to 74.82%. Clearly, within the range of JRC from 13.05 to 5.26 and a temperature range of 20 to 90 °C, the influence of fracture roughness on nonlinear flow behavior exceeds that of temperature. At a confining pressure of 60 MPa and a hydraulic gradient of 200 MPa/m, as the temperature rises from 20 to 90 °C, the F_0 value of Specimen 1 increases from 4.32% to 10.72%, while that of Specimen 3 increases from 23.09% to 28.48%. Compared to a confining pressure of 30 MPa, the effects of both temperature and roughness on nonlinear flow behavior are significantly reduced. This is mainly due to the obvious narrowing

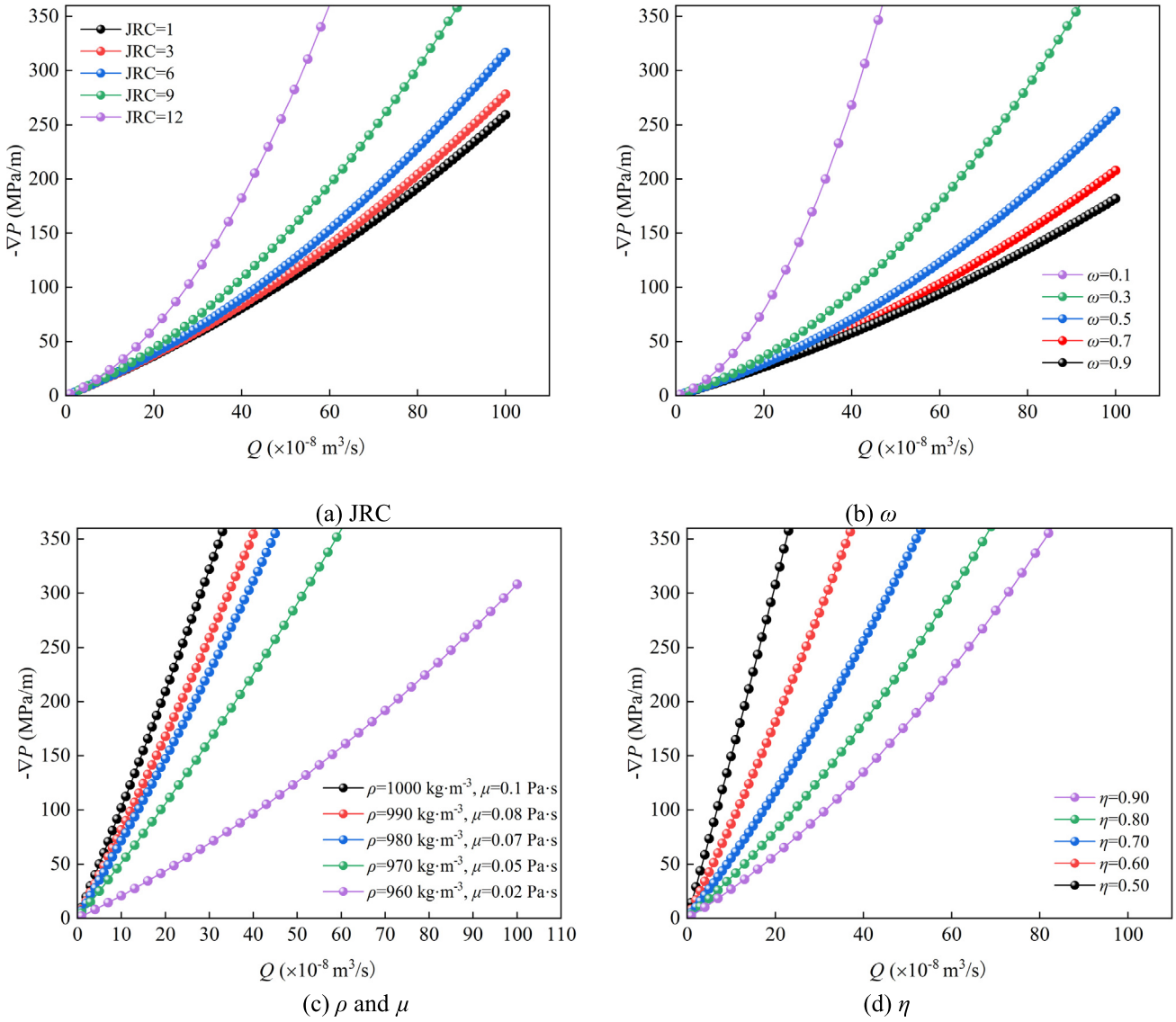

Fig. 15. Local sensitivity analysis of parameters of the improved Forchheimer equation under a confining pressure of 30 MPa.

of the flow channel at 60 MPa, where the flow paths are severely restricted by the confining pressure, thereby diminishing the nonlinear characteristics.

5.4. Future work

Although the model proposed in this study offers new insights into the nonlinear flow behavior of rough single fractures under coupled HTHM conditions, several limitations remain that warrant further investigation. To enhance the model's applicability and improve its practical value in broader fields such as geotechnical engineering and energy development. Future research should focus on the following aspects:

(1) Flow behavior when the seepage pressure approaches or reaches the confining pressure. Although this study includes seepage pressure conditions as high as 60 MPa, the corresponding confining pressure was maintained at 120 MPa, resulting in sufficiently large effective stress. However, in certain deep subsurface engineering scenarios, particularly in petroleum engineering, abnormally high pore pressures may occur, where the seepage pressure approaches or even equals the confining pressure, leading to nearly zero effective stress. Under such extreme conditions, fluid flow behavior within rock fractures remains unclear and requires further investigation.

(2) Flow behavior in poorly matched fracture surfaces under coupled HTHM conditions. In this study, fracture surfaces were produced by splitting intact rock cores, resulting in relatively well-matched fracture pairs with minimal geometric evolution under varying confining pressure conditions. In nature or engineering practice, there are also cases of poor matching of fracture surfaces, resulting in more complex contact states and geometric deformations caused by confining pressure. Future work should consider using technologies such as 3D printing to fabricate fracture specimens with controlled roughness but low matching degrees, allowing systematic investigation of fluid flow behavior under extreme coupled conditions.

(3) Flow behavior at higher temperatures and involving multiphase fluids. To avoid fluid phase transitions during testing, the temperature range in this study was limited to 20–90 °C,

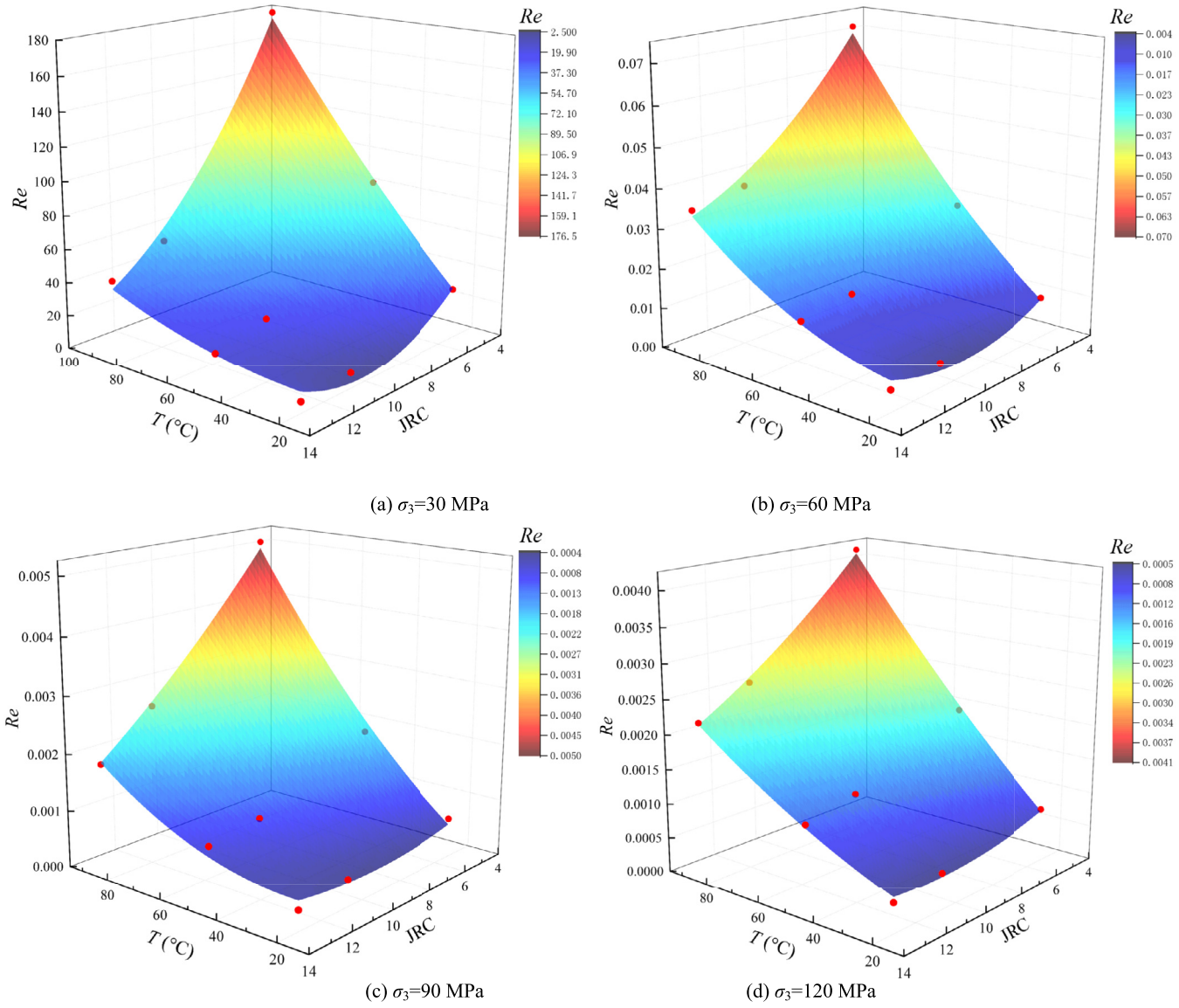

Fig. 16. Variation of Reynolds number with temperature and roughness under different confining pressures.

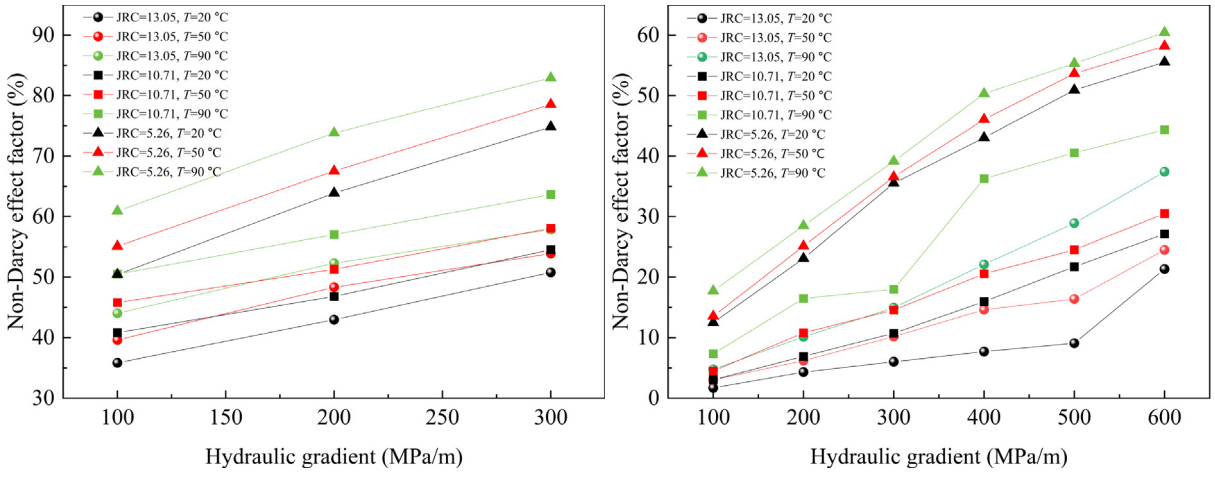

Fig. 17. Variation of non-Darcy effect factor F_0 of a single rock fracture with temperature under different hydraulic gradients.

which is representative of deep tunnel excavation conditions. However, this range does not fully capture the high-temperature environments typical of petroleum extraction and geothermal development. Future research should focus on designing experimental systems capable of operating at higher temperatures to investigate the coupled flow behavior of multiphase fluids under HTHM conditions.

6. Conclusions

To gain a comprehensive understanding of the seepage behavior of fractured rock at different depths, a self-developed multi-field coupling experimental system was employed to conduct seepage experiments. The tests covered a temperature range of 20 to 90 °C confining pressures from 30 to 120 MPa, and seepage pressures from 5 to 60 MPa on single fractured rocks with varying roughness. This study elucidates the influence of multi-factor coupling on the flow behavior of single fractured rock. Furthermore, an improved Forchheimer equation is proposed to accurately characterize the flow behavior of single fractured rock with varying roughness under HTHM conditions. The main conclusions are as follows:

(1) Confining pressure significantly alters flow behavior by reducing the hydraulic aperture. As confining pressure increases from 30 to 120 MPa, flow behavior transitions from Forchheimer flow to low-velocity nonlinear flow. At lower confining pressures (<60 MPa), the increase in seepage pressure induces inertial effects, resulting in Forchheimer flow behavior. When the confining pressure reaches 60 MPa, the hydraulic aperture decreases to the sub-micrometer scale, causing the flow behavior to shift toward low-velocity nonlinear.

(2) The influence of seepage pressure on fluid flow behavior diminishes as the confining pressure increases. At relatively low confining pressures (<60 MPa), an increase in relative seepage pressure from 16.6% to 50% leads to a significant expansion of the hydraulic aperture (5%). However, when the confining pressure exceeds 60 MPa, the hydraulic aperture increases by less than 5% under the same relative seepage pressure change.

(3) The effects of temperature and fracture surface roughness on fluid flow behavior vary with confining pressure. When the JRC of fractured rocks ranges from 13.05 to 5.26, the temperature varies between 20 and 90 °C and the confining pressure is below 60 MPa, roughness dominates flow behavior, while its influence diminishes with increasing confining pressure due to aperture reduction. Additionally, under the same seepage pressure, the effect of temperature on the volumetric flow rate of fractured rocks increases as JRC decreases, while the influence of roughness on volumetric flow rate is not significantly affected by temperature.

(4) Reynolds number and non-Darcy effect factor are confining pressure-dependent. Reynolds number increases with temperature and decreases with roughness, but both effects weaken under higher confining pressures. The non-Darcy effect factor is significantly influenced by confining pressure, with Forchheimer flow being more likely to occur at 30 MPa. Temperature-induced viscosity reduction and roughness-induced flow path tortuosity promote nonlinear flow through different mechanisms.

Acknowledgments

This work was supported by the National Natural Science Foundation of China (Nos. 52034010 and 52479113), the Natural Science Foundation of Shandong Province, China (No. ZR2024ME165), and the Postgraduate Education and Teaching Reform Project of China University of Petroleum (East China) (No. YJG2024005).

References

[1] Jiang MM, Liu QY. Geochemical characteristics of ultra-deep natural gases. Org Geochem 2025;203:104964.
[2] Wu MY, Chang X, Guo YT, Liu JJ, Yang CH, Suo Y. Advances, challenges, and opportunities for hydraulic fracturing of deep shale gas reservoirs. Adv Geo-Energy Res 2025;15(1):1–4.
[3] Zhu DY, Liu QY, Wang JB, Peng ST, You DH, Zhang JT, Ding Q, Wu CY. Differential fault-fluid alterations and reservoir properties in ultra-deep carbonates in the Tarim Basin. NW China. Appl Geochem 2024;170:106084.
[4] Wen ZX, Wang JJ, Wang ZM, He ZJ, Song CP, Chen RY, Liu XB, Ji TY, Li ZX. Analysis of the current status of global oil, gas, and associated resources exploration in 2023. Petrol Explor Dev 2024;51(6):1465–79.
[5] Liao QZ, Wang B, Chen X, Tan P. Reservoir stimulation for unconventional oil and gas resources: recent advances and future perspectives. Adv Geo-Energy Res 2024;13(1):7–9.
[6] Wang WY, Pang XQ, Wang YP, Chen ZX, Jiang FJ, Chen Y. Quantitative prediction model for the depth limit of oil accumulation in the deep carbonate rocks: A case study of Lower Ordovician in Tazhong area of Tarim Basin. Petrol Sci 2024;21(1):115–24.
[7] Yu BC, Zhang DM, Xu B, Li MH, Liu C, Xiao WJ. Experimental study on the effective stress law and permeability of damaged sandstone under true triaxial stress. Int J Rock Mech Min Sci 2022;157:105169.
[8] Liu RC, Li B, Jiang YJ. Critical hydraulic gradient for nonlinear flow through rock fracture networks: The roles of aperture, surface roughness, and number of intersections. Adv Water Resour 2016;88:53–65.
[9] Shu B, Zhu RJ, Elsworth D, Dick J, Liu S, Tan JQ, Zhang SH. Effect of temperature and confining pressure on the evolution of hydraulic and heat transfer properties of geothermal fracture in granite. Appl Energy 2020;272:115290.
[10] Gan L, Liu Y, Xu T, Xu L, Ma HY, Xu WC. Experimental investigation of the seepage characteristics of a single fracture in limestone with different roughness and seepage fluids. J Hydrol 2023;622:129699.
[11] Wu S, Gao K, Feng Y, Huang XL. Influence of slip and permeability of bedding interface on hydraulic fracturing: A numerical study using combined finite-discrete element method. Comput Geotech 2022;148:104801.
[12] Tian ZX, Zhang WS, Dai CQ, Zhang BL, Ni ZQ, Liu SJ. Permeability model analysis of combined rock mass with different lithology. Arab J Geosci 2019;12(24):755.
[13] Barton N, Choubey V. The shear strength of rock joints in theory and practice. Rock Mech 1977;10(1):1–54.
[14] Tao GL, Peng P, Chen QS, Nimbalkar S, Huang Z, Peng YJ, Zhao W. A new fractal model for nonlinear seepage of saturated clay considering the initial hydraulic gradient of microscopic seepage channels. J Hydrol 2023;625:130055.
[15] Maerz NH, Franklin JA, Bennett CP. Joint roughness measurement using shadow profilometry. Int J Rock Mech Min Sci Geomech Abstr 1990;27(5):329–43.
[16] Todhunter LD, Leach RK, Lawes SDA, Blateyron F. Industrial survey of ISO surface texture parameters. CIRP J Manuf Sci Technol 2017;19:84–92.
[17] Li YZ, Cui Y, Li YC, Gan YX. Analysis and prediction of contact characteristics of rock fracture surfaces under normal loading. J Struct Geol 2024;180:105086.
[18] Wang CS, Liu RC, Jiang YJ, Wang G, Luan HJ. Effect of shear-induced contact area and aperture variations on nonlinear flow behaviors in fractal rock fractures. J Rock Mech Geotech Eng 2023;15(2):309–22.
[19] Qian JZ, Chen Z, Zhan HB, Guan HC. Experimental study of the effect of roughness and Reynolds number on fluid flow in rough-walled single fractures: a check of local cubic law. Hydrol Process 2011;25(4):614–22.
[20] He XP, Sinan M, Kwak H, Hoteit H. A corrected cubic law for single-phase laminar flow through rough-walled fractures. Adv Water Resour 2021;154:103984.
[21] Sukop MC, Huang HB, Alvarez PF, Variano EA, Cunningham KJ. Evaluation of permeability and non-Darcy flow in vuggy macroporous limestone aquifer samples with lattice Boltzmann methods. Water Resour Res 2013;49(1):216–30.
[22] Zimmerman RW, Bodvarsson GS. Hydraulic conductivity of rock fractures. Transp Porous Medium 1996;23(1):1–30.
[23] Renshaw CE. On the relationship between mechanical and hydraulic apertures in rough-walled fractures. J Geophys Res Solid Earth 1995;100(B12):24629–36.

[24] Schrauf TW, Evans DD. Laboratory studies of gas flow through a single natural fracture. Water Resour Res 1986;22(7):1038–50.
[25] Spiridonov D, Vasilyeva M. Non-local multi-continuum method (NLMC) for Darcy–Forchheimer flow in fractured media. J Comput Appl Math 2024;438:115574.
[26] Zhang YX, Yan HJ, Yang SL, Deng H, Peng X, Chen ZX. Effects of temperature on seepage capacity for a multi-type ultra-deep carbonate gas reservoir. J Nat Gas Geosci 2023;8(2):153–67.
[27] Ma D, Duan HY, Li XB, Li ZH, Zhou ZL, Li TB. Effects of seepage-induced erosion on nonlinear hydraulic properties of broken red sandstones. Tunn Undergr Space Technol 2019;91:102993.
[28] Altawati F, Emadi H. Effects of cyclic cryogenic treatment on rock physical and mechanical properties of Eagle Ford shale samples - An experimental study. J Nat Gas Sci Eng 2021;88:103772.
[29] Liang XF, Meng T, Feng G, Zhao GH, Wang ZX, Liu PT. Evolution of permeability and pore structure of salt rock and its self-healing mechanism under coupled thermo-hydro-mechanical environment. J Energy Storage 2023;66:107476.
[30] Meng T, Zhang ZJ, Taherdangkoo R, Zhao GH, Butscher C. Temperature-dependent evolution of permeability and pore structure of marble under a high-temperature thermo-hydro-mechanical coupling environment. Acta Geotech 2024;19(9):5967–88.
[31] Li MY, Wu ZJ, Weng L, Zhang FS, Zhou Y, Wu Y. Cross-scale analysis for the thermo-hydro-mechanical (THM) effects on the mechanical behaviors of fractured rock: integrating mesostructure-based DEM modeling and machine learning. Eng Fract Mech 2024;306:110204.
[32] Yi W, Huang SX, Rao QH, Li Z, Huang DY, Ma Y, Liu ZL. Cracking behaviors and mechanism of pre-cracked rock specimens under coupled THM fields with chemical processes. Case Stud Constr Mater 2024;20:e02758.
[33] Zhang W, Wang D, Wang ZL, Guo TK, Wang CG, He JY, Zhang L, Zheng P, Qu ZQ. Study on permeability evolution and damage mechanism along the EGS fracture in heat mining stage under thermal stress/cracking. Geotherm Energy 2023;11(1):31.
[34] Wu RY, Chen SW, Wang GB, Zhu YH, Lan XD. Development and application of a thermo-hydro-mechanical coupling test system for a single rock fracture. Measurement 2025;242:116197.
[35] Meng T, Wang TT, Guo K, Zhang DK. Study of mode II fracture characteristics and roughness in salt rock after treatment coupled thermo-hydro-mechanical environment. Eng Fract Mech 2023;291:109572.
[36] Wu FB, Zhang DK, Ma LF, Meng T, Zhao GH, Liu PT, Zhang ZJ, Taherdangkoo R, Bustscher C. Thermo-hydro-mechanical (THM) evolution law and development of permeability and pore structure of enhanced geothermal systems at ultra-high temperatures. Geothermics 2021;97:102253.
[37] Huang J, Song ZL, Liao ZW, Zhao WC, Wang D. Quantification of cracks and the evolution of permeability for reservoir rock under coupled THM: Equipment development and experimental research. Geomech Geophys Geo Energy Geo Resour 2020;6(4):63.
[38] Geng SY, Zhou YH, Geng M, Wen ZG, Bai FF, Bai YY. New insights into the identification and characterization of Darcy-to-Forchheimer flow transitions in rough fractures. J Hydrol 2025;659:133252.
[39] Kumari WGP, Ranjith PG. Experimental and numerical investigation of the flow behaviour of fractured granite under extreme temperature and pressure conditions. Sustainability 2022;14(14):8587.
[40] Abddaim E, Sakami S, El Hassnaoui A, Boukhattem L. Impact of temperature on chemical, thermo-physical, and mechanical properties of four rock materials for sensible thermal energy storage. J Energy Storage 2024;89:111602.
[41] Barton N, Bandis S, Bakhtar K. Strength, deformation and conductivity coupling of rock joints. Int J Rock Mech Min Sci Geomech Abstr 1985;22(3):121–40.
[42] Walsh JB. Effect of pore pressure and confining pressure on fracture permeability. Int J Rock Mech Min Sci Geomech Abstr 1981;18(5):429–35.
[43] Yu X, Zhang T, Yang K, Yu F, Liu Y, Tang M. Quantitative characterization of seepage behavior in rough fracture considering hydromechanical coupling effect: An experimental study. Acta Geophys 2023;71(5):2245–64.
[44] Chen YD, Liang WG, Lian HJ, Yang JF, Nguyen VP. Experimental study on the effect of fracture geometric characteristics on the permeability in deformable rough-walled fractures. Int J Rock Mech Min Sci 2017;98:121–40.
[45] Floquet N, Vielzeuf D, Heresanu V, Laporte D, Perrin J. Synchrotron high-resolution XRD and thermal expansion of synthetic Mg calcites. Phys Chem Miner 2020;47(11):48.
[46] Xu P, Li ZQ, Wang JQ, Chen Q, Qiu SX. A new fractal pore-throat chain model for non-Darcy flow through porous media. Adv Water Resour 2024;192:104782.
[47] Arianfar A, Ramezanzadeh A, Khalili M. Numerical modeling of closure effect of natural fracture surfaces of rock on behavior of fluid flow. Bull Eng Geol Environ 2021;80(3):2335–48.
[48] Ali F, Zaib A, Abbas M, Anitha G, Loganathan K, Reddy GR. Radiative flow of cross ternary hybrid nanofluid (MoS_2, TiO_2, Ag/CMC-water) in a Darcy Forchheimer porous medium over a stretching cylinder with entropy minimization. Heliyon 2024;10(14):e34048.
[49] Konzuk JS, Kueper BH. Evaluation of cubic law based models describing single-phase flow through a rough-walled fracture. Water Resour Res 2004;40(2):W02402.
[50] Qian X, Xia CC, Gui Y, Zhuang XQ, Yu QF. Study on flow regimes and seepage models through open rough-walled rock joints under high hydraulic gradient. Hydrogeol J 2019;27(4):1329–43.